Evidence of Mineral Phase and Eutectic Chemistry as Dominant Factors Affecting Deposition of Heterogeneous Mineral Dust in an Impingement Coolant Jet

Thesis

Presented in Partial Fulfillment of the Requirements for the Degree Master of Science in the Graduate School of The Ohio State University

By

Eric Patrick Nied, BSE

Graduate Program in Aerospace Engineering

The Ohio State University

2022

Thesis Committee

Jeffrey P. Bons, Advisor

Michael G. Dunn

Abstract

AFRL02 is a ubiquitous test dust in the field of particle deposition in gas turbine engines. The traditional recipe for AFRL02 is 34 mass percent quartz, 30 mass percent gypsum, 17 mass percent aplite, 14 mass percent dolomite, and five mass percent halite. In the present study, albite was substituted for aplite, and hematite was added for certain tests. This thesis seeks to unpack the synergies that exist between minerals during deposition of the heterogeneous AFRL02 mixture in gas turbine engines and demonstrate that incoming mineral phases and eutectic chemistry are major factors in the deposition phenomenon through their relation to eutectic melt formation and subsequent deposit properties, such as melting temperature, viscosity, and surface tension. Capture efficiency measurements, deposit morphology analyses, and X-ray diffraction results are reported and discussed for deposition experiments performed with the Impingement Deposition Rig at The Ohio State University. In each experiment, one gram of a mineral dust (0-10μm particle diameter distribution) was injected into an 894K, 57m/s coolant flow impinging normally on a Hastelloy X plate with a surface temperature of 1033K, 1144K, or 1255K. Besides AFRL02, single mineral dusts, dual mineral dusts, and AFRL02-like dust blends lacking in one mineral were tested. The results of the experiments elucidate that the deposition behavior of single minerals cannot explain the composite deposition of heterogeneous mixtures of minerals. For example, gypsum had the highest capture

efficiency of any single mineral in ARFL02, and yet removing gypsum from AFRL02 counterintuitively raised the capture efficiency of that blend when compared to AFRL02. Quartz was found to erode albite deposits but stick to and build upon dolomite and halite deposits, even though quartz did not deposit significantly as a single mineral. Quartz also chemically reacted with gypsum and dolomite to form wollastonite and diopside, respectively. Finally, it was found that the capture efficiency of each blend increased with plate temperature, but not according to the same trend. Results are interpreted through the lens of CaO-MgO-Al_2O_3-SiO_2 eutectic chemistry – influenced by advances in the field of agglomeration in Fluidized Bed Combustion – and credible explanations of deposition behavior based on mineral phase and eutectic chemistry are put forward. This thesis concludes by revisiting a handful of well-known, key trends in the field of deposition in gas turbine engines and explaining how mineral chemistry might manifest itself in each of these trends.

Acknowledgments

I have been blessed throughout my life by the unconditional love and support of my parents, Gary J. and Kay Nied, and brother, Benjamin Nied. Any modest success I achieve in life can be traced back directly to them, and I am truly grateful. Gary M. Nied and Stephen DiSalvio selflessly edited my graduate school application personal statements, which helped me gain admission into graduate school. I would also like to thank my wife, Yu Xin. In November 2019 we parted ways in Chongqing, China, not realizing a major, global pandemic that would separate us for almost two years was about to strike a month later. Her love, support, and patience in the face of hardship could inspire a modern love novel or movie. I am also thankful to my advisor, Dr. Jeffrey Bons. I had reluctantly decided not to attend OSU when I had the great fortune of meeting Dr. Bons. He not only changed the course of my life that day by convincing me to come to OSU, but continued to change me each and every day by setting an example of how to be a great scientist and human being. My classmates and coworkers have supported me in the laboratory, classroom, and machine shop. I am especially grateful to Blair Peterson, Ian Potts, Dr. Chris Bowen, Jiaxuan Han, Roger Zeits, Chihsiu Lo, Nathanael Wendel, Semo Slaoui, Alex Spens, Dr. Rajat Saksena, Evan McFadden, Collin Rambacher, Dr. Wenbo Zhu, John Muhl, Patrick Brandt, Anthony Pisano, Josh Gueth, Ken Fout, and Won Sik Shin. Other mentors who have helped me on my journey at OSU include Dr.

Mo Samimy, Dr. Sandip Mazumder, Dr. Clarissa Belloni, Dr. Louis Christensen, Dr. Lian Duan, Dr. Nandini Trivedi, Dr. Hendrik Colijn, and Dr. Michael Dunn. I would also like to thank previous mentors. Dr. Charles Rosenblatt, my undergraduate research advisor, inspired me to return to graduate school with his generous acknowledgement of me in a paper published on the Rayleigh-Taylor fluid instability, and in many ways has continued to advise me over ten years after his formal obligation ended. Johan Steenkamp and Bertus Heymans of CEC Controls Company, Inc. taught me the practical side of engineering not taught in school. A group of lifelong friends from my hometown of Wadsworth, Ohio have also acted as a support network for me during the two pandemic-smudged years of graduate school. They know who they are and that their support is appreciated; I especially thank Dr. Joseph Ozbolt for the many late-night math and physics conversations we had under the stars growing up.

Vita

2007 .....Wadsworth High School

2012.....B.S.E. Engineering Physics, Case Western Reserve University

2016-2019.....International Computer Integrated Manufacturing Engineer, CEC Controls Company, Inc.

2020 to present .....Graduate Research Associate, Department of Mechanical and Aerospace Engineering, The Ohio State University

Fields of Study

Major Field: Aerospace Engineering

Table of Contents

Abstract ii

Acknowledgments iv

Vita vi

List of Tables x

List of Figures xi

Chapter 1. Introduction 1

Chapter 2. The Phenomenon of Deposition and Characterization of Deposits 9

Chapter 3. Scope of Work 13

Chapter 4. Literature Review Part I: Variables Affecting Particle Deposition in Gas Turbine Engines 17

Effect of Temperature 17

Effect of Particle/Flow Velocity 18

Effect of Particle Size 20

Effect of Particle Shape 21

Effect of Pressure 22

Chapter 5. Literature Review Part II: Chemistry's Effect on Deposition 24

Chapter 6. Literature Review Part III: Introduction to Fluidized Bed Combustion and Its Contribution to Knowledge of Mineral Eutectics 26

Chapter 7. Literature Review Part IV: Impingement Flows 30

Flow Field 30

Heat Transfer 32

Impingement Arrays in Gas Turbine Engines 32

Chapter 8. Experimental Set-up and Procedure 34

Summary of Experiment 34

The Declumper 37

Dust Milling and Sizing 38

Chapter 9. Methods of Data Collection and Analysis 40

Capture Efficiency 40

X-Ray Diffraction 41

Deposit Morphology 43

Chapter 10. Results and Analysis 46

Single Mineral Dust Tests Results 46

AFRL02 Dust Tests Results 50

Dual Mineral Dust Tests Results 55

Sequential Dual Mineral Dust Tests Result 56

Simultaneous Dual Mineral Dust Tests Results 57

Blends 1-6 Tests Results 59

Supplemental Studies 65

Alumina Results 65

ARD Results 67
Chapter 11: Discussion 71
Generalizations and Limitations 75
Another Look at Factors Which Affect Deposition Through the Lens of Chemistry .. 76
Effect of Temperature 76
Effect of Particle/Flow Velocity 77
Effect of Pressure 78
Effect of Particle Size 79
Effect of Particle Shape 79
Dust Versus Volcanic Ash 80
Observations of Deposit Morphology 81
Deposit Cone Growth 81
Molten Deposits 84
The Gap Region 85
Deposit Erosion 87
Chapter 12: Conclusions 88
References 90

List of Tables

Table 1: Oxide content of ARD as reported by PTI 7

Table 2: Mineral content of AFRL02 8

Table 3: Dust blends used in this study 15

Table 4: Test conditions..... 35

Table 5: New minerals formed in AFRL02 deposits..... 54

Table 6: XRD results, given in weight percentage, for analyzed deposits of blends 1-6 . 64

List of Figures

Figure 1: An MV-22B Osprey kicks up dust and sand into the air [3]. 2

Figure 2: Volcanic ash deposits on turbine NGVs from British Airways Flight 9 [4] 3

Figure 3: Trend of takeoff turbine entry temperature with time [5] 4

Figure 4: NASA image of the 2020 Saharan dust storm drifting over the Atlantic [7] 5

Figure 5: A plume of smoke and ash rises from a volcano [8] 5

Figure 6: A simple schematic of the deposition phenomenon 10

Figure 7: Flow field for round jet impinging upon a flat plate [43] 31

Figure 8: Employment of impingement cooling in turbine blades and combustor liners of gas turbine engines [44] 33

Figure 9: Impingement Deposition Rig 35

Figure 10: Cumulative volume statistics for mineral dusts used in this study 39

Figure 11: Bragg's Law, governing principle of XRD [46] 42

Figure 12: Deposits formed at 1144K surface temperature (a) hematite (b) AFRL02 43

Figure 13: Capture efficiencies of single mineral dusts 46

Figure 14: Representative pictures of each single mineral dust's deposits; Column 1 = 1033K, Column 2 = 1144K, Column 3 = 1255K 47

Figure 15: XRD result for dolomite deposit at 1255K plate temperature 49

Figure 16: AFRL02 deposits at (a) 1033K (b) 1144K and (c) 1255K plate surface temperatures 50

Figure 17: Capture efficiency results for experimental and hypothetical AFRL02 compared to single mineral capture efficiency results 52

Figure 18: Experimental and hypothetical XRD results for AFRL02 deposits at three plate surface temperatures 53

Figure 19: Cumulative volumes of sequential dual mineral deposits at 1144K plate surface temperature 56

Figure 20: Simultaneous dual mineral capture efficiencies at 1144K plate surface temperature 58

Figure 21: XRD results for blend 9 (dolomite-quartz) and blend 7 (gypsum-quartz) simultaneous dual mineral tests and plate temperature = 1144K 59

Figure 22: Capture efficiency results for all minerals and blends at all plate surface temperatures 60

Figure 23: Representative pictures of blends' 1-6 deposits at all three plate temperatures; Column 1 = 1033K, Column 2 = 1144K, Column 3 = 1255K 63

Figure 24: Representative alumina deposit at 1144K plate surface temperature 66

Figure 25: Single mineral capture efficiencies including alumina 66

Figure 26: Representative pictures of ARD deposits at constant (1144K) plate surface temperature and varying (a) 839K, (b) 894K, (c) 950K flow temperature 68

Figure 27: Representative pictures of ARD deposits at constant (894K) flow temperature and varying (a) 1033K, (b) 1144K, (c) 1255K plate surface temperature 68

Figure 28: ARD capture efficiencies at various flow temperatures 69

Figure 29: ARD capture efficiencies at various plate surface temperatures 69

Figure 30: Close up of an albite deposit at 1033K plate surface temperature showing the wavefronts of layer formation 82

Figure 31: PSV image of albite deposit during dust delivery showing layered growth; direction of propagation is inwards, towards the peak 83

Figure 32: An ARD central deposit split in two parallel to cone surface, revealing layered structure of cone 83

Figure 33: A molten drop detaches from central deposit and moves outwards under influence of shear flow..... 85

Chapter 1. Introduction

Gas turbine engines are air-breathing propulsion devices: they rely on oxygen in the air entering the engine from the atmosphere to combust on-board fuel. Not requiring an on-board oxidizer – in contrast to, for example, rocket engines – benefits aircraft employing gas turbine engines by affording them a considerable weight-savings and increase in safety. Even without an oxidizer on-board, fuel is often 20-40% of a commercial aircraft's maximum weight at takeoff [1]. One major disadvantage of gas turbine engines is that, along with the air they breathe, they ingest fine particulates (and sometimes an unfortunate bird) suspended in that air. There are a few mechanisms by which these particulates can cause damage to the engine: 1) erosion of leading edges due to highly energetic collisions between non-molten particles and engine components; 2) formation of deposits which block coolant flows (leading to overheating of the engine) and main line flows (decreasing flow area and possibly causing stall or surge); 3) chemical infiltration of molten deposits into thermal barrier coatings, leading to spallation of the coatings and reduced part lifetime of the surfaces those coatings are meant to protect.

The effects of these fine particulates can be devastating for both commercial and military aircraft. In 1982, British Airways Flight 9's Boeing 747 took off from Kuala Lumpur, Malaysia into a cloud of volcanic ash causing the temporary failure of all four engines. The 2010 eruption of the volcano Eyjafjallajökull in Iceland caused large

financial losses and a logistical nightmare for flights across Europe and North America. And even more recently, in 2015, a Navy MV-22B Osprey crashed during a training exercise in Hawaii, killing both pilots. The official cause of the crash was deemed a combination of brownout conditions, blocking the pilots' view of the landing spot, and stall in the left engine – both caused by the large cloud of sand and dust kicked up by the aircraft's tiltrotors [2]. Additionally, particulates which enter the cabin via compressor bleed to the cabin may cause serious lung problems for the humans which inhale them.

Figure 1: An MV-22B Osprey kicks up dust and sand into the air [3].

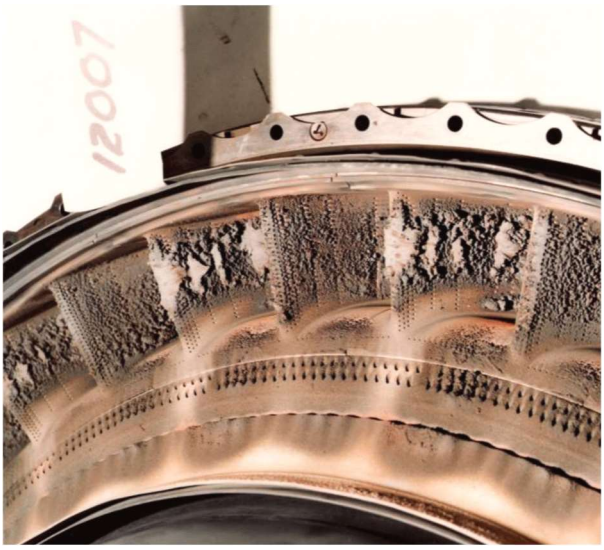

Figure 2: Volcanic ash deposits on turbine NGVs from British Airways Flight 9 [4]

The historical and current industry trend in gas turbine engines is an unceasing drive to increase fuel efficiency in order to reduce fuel costs and carbon emissions. By burning the same amount of fuel at a hotter temperature, more energy can be extracted by the turbine and an increase in thrust is achieved. This makes clear that the problem of deposition is not going away any time soon and, in fact, will be exacerbated as temperatures in the combustor and turbine increase. For as engine temperatures increase, softening, melting, decomposition and reaction temperatures of more and more mineral particulates are surpassed. It also means that the melting temperatures of the materials which compose the engine themselves are surpassed, which makes the optimal operation of cooling schemes even more critical. If mineral deposits block coolant flows and cause overheating, risks include the melting of engine components during operation.

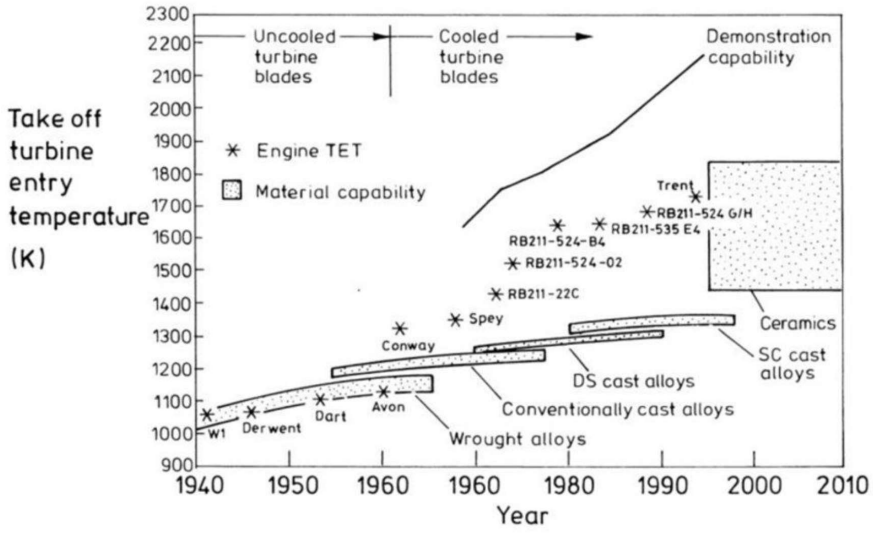

Figure 3: Trend of takeoff turbine entry temperature with time [5]

One might ask: how does this fine particulate dust get into the atmosphere? Volcanic eruptions and Saharan dust storms are dramatic examples, but by no means the only ones. Industrial air pollution, salty sea spray, and arid landscapes are all common origins of fine particulates in the atmosphere. Micron-sized particles have large surface area-to-volume ratios, meaning two-dimensional lift forces dominate over inertial forces such as weight force due to gravity, lifting particles high into the atmosphere. Consider that a phenomenon as common as rain is understood to be the result of particles in the atmosphere acting as nucleation points for water condensation [6].

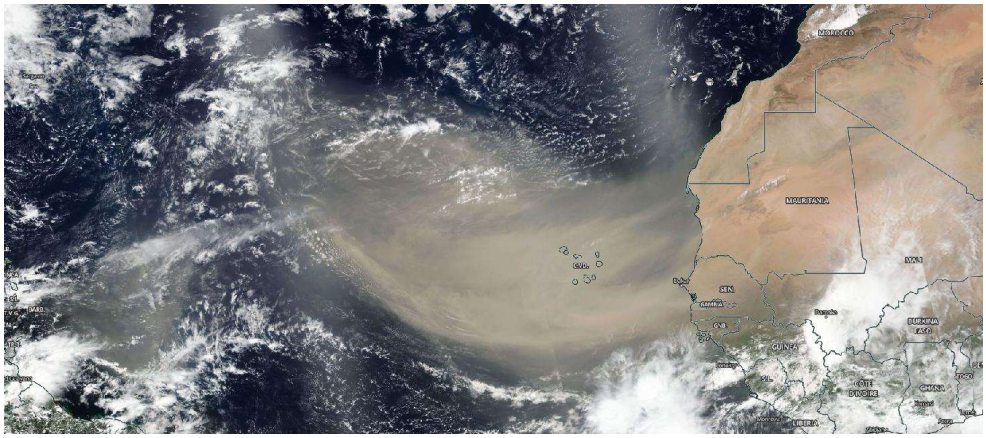

Figure 4: NASA image of the 2020 Saharan dust storm drifting over the Atlantic [7]


Figure 5: A plume of smoke and ash rises from a volcano [8]

With such a large variety of sources, it is no surprise that the chemistry of these particulates is equally variable. In an unclassified report for the Australian Department of Defense, Wood et al. reported characterizations of 21 dust, dirt, and ash samples collected from aircraft engine components or the ground from locations as diverse as New Zealand, Iraq, USA, and Chile. Although all samples were dominated by silicate minerals, including quartz, they nevertheless showed heterogeneities in mineral and elemental composition [9].

Despite heterogeneous mineral chemistry being an obvious variable in the deposition phenomenon, researchers have not yet fully captured its role. One reason is the inherent lack of control in characterizing its effects in the real world. No two flights will follow exactly the same flight pattern and be exposed to exactly the same concentrations of chemically equivalent dust or ash. For this reason, "standardized" test dusts were developed as a basis for comparison between deposition experiments. The two most well-known are Arizona Road Dust (ARD) and Air Force Research Laboratory Test Dust (AFRL02). ARD is harvested from topsoil in the Salt River Valley in Arizona by Powder Technologies Incorporated (PTI), who also helped author ARD's ISO standard [10]. Its exact mineral content varies, as would be expected of any natural dust, even when harvested from within the same valley. Therefore, the ISO standard only dictates the oxide content. This is given in Table 1, as supplied by PTI. The author's own X-ray Diffraction (XRD) analysis on a purchased batch of ARD revealed it to be about 40 mass percent quartz, 33 mass percent clay minerals, such as montmorillonite, illite, kaolinite, and muscovite, 20 mass percent feldspar, including albite, microclase, and anorthite, and

seven mass percent calcite. (An unfortunate reality in gas turbine literature is that often just the oxide content is reported for ARD, which misses the point that SiO_2 which exists as pure quartz will deposit very differently than SiO_2 contained in a more complex silicate mineral with alkali or alkaline-earth oxides.) The other common test dust is AFRL02, which was named after the Air Force Research Laboratory in Dayton, Ohio, who conceived of it [11]. Being a laboratory-made test dust means its composition is well known to the exact percent. It is comprised of 34 mass percent quartz, 30 mass percent gypsum, 17 mass percent aplite (a combination of quartz and the alkali felspars albite and microclase), 14 mass percent dolomite, and five mass percent halite, as reiterated in Table 2.

Table 1: Oxide content of ARD as reported by PTI

Oxide	Mass Percentage Range
SiO_2	68-76
Al_2O_3	10-15
Fe_2O_3	2-5
Na_2O	2-4
CaO	2-5
MgO	1-2
TiO_2	0.5-1.0
K_2O	2-5

Table 2: Mineral content of AFRL02

Mineral	Common Name	Mass Percentage
SiO_2	Quartz	34
$CaSO_4 \cdot 2H_2O$	Gypsum	30
$SiO_2 + (K,Na)AlSi_3O_8$	Aplite	17
$CaMg(CO_3)_2$	Dolomite	14
NaCl	Halite	5

The test dust which is the focus of this thesis is AFRL02. AFRL02 was developed in an attempt to reverse engineer ingested dust from glassy deposits scraped from real engine components, often known as CMAS (CaO-MgO-Al_2O_3-SiO_2) deposits. Many jet engine manufacturers and end users are required to document how their engines function (or fail to function) when subjected to AFRL02-laden air. However, several important questions about this test dust's chemistry remain open: Do minerals all deposit independently or are there synergies between them? Is bulk, elemental chemistry most important, or do mineral phases matter as well? Are there any generalizations that can applied to any heterogeneous mixture of minerals? The answers to these questions are explored in the following pages. Heterogeneous mineral chemistry does turn out to be an important factor in deposition tests in an impingement coolant flow. Eutectic mixtures of minerals directly determine critical temperatures – such as softening and melting temperatures – and viscosity and surface tensions of deposits, which are some of the most important factors to consider when discussing deposition. However, the phases which these minerals enter the engine are equally important.

Chapter 2. The Phenomenon of Deposition and Characterization of Deposits

The simplest model of the phenomenon of particle deposition in gas turbine engines is the following: a mineral particle of some fixed size and shape, with some kinetic energy and temperature, and some material-dependent properties, such as melting temperature, Poisson's ratio, Young's modulus, hardness, etc., travels towards and collides with a hot surface in an engine. Its collision with the surface is neither perfectly elastic nor inelastic. After the collision, if the particle's rebound kinetic energy is enough to overcome surface forces of attraction between the particle and the component, it does not deposit, and travels away from the surface. However, if the surface forces (including van der Waals, electrostatic, and capillary forces) are strong enough to overcome the rebound kinetic energy, the particle deposits. It is a balance between these two energies, the rebound kinetic energy and the surface free energy. The surface energy need not be great if the collision is highly inelastic. A schematic can be found in Figure 6. During the initial stages of deposition, the surface forces of attraction are adhesive forces between the particle and engine surface. As a layer of deposit builds, however, newly incoming particles will collide with an existing deposit, and the forces become cohesive forces between the particle and mineral deposit.

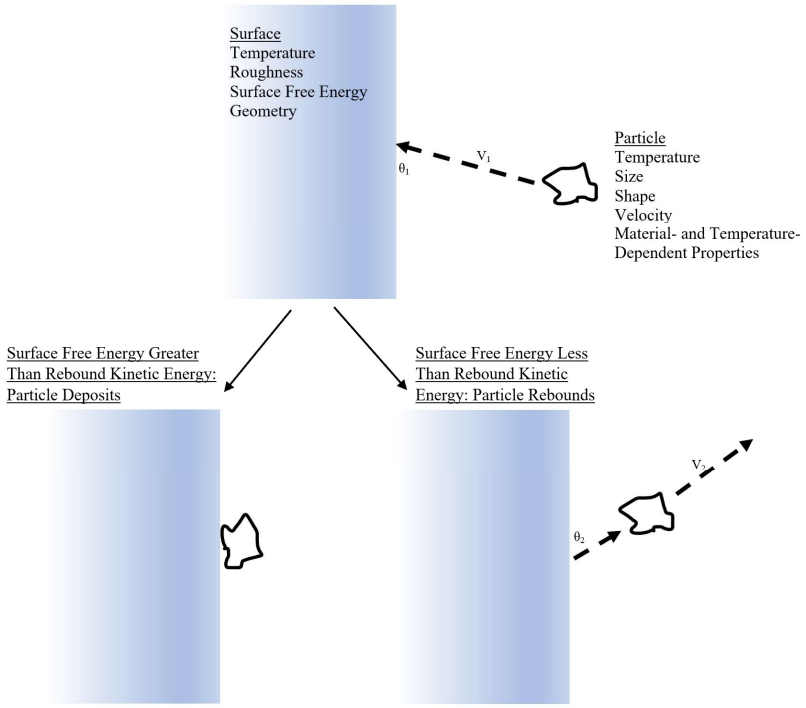

Figure 6: A simple schematic of the deposition phenomenon

Along with standardized test dusts, there needs to be standard metrics to characterize deposits so that scientists studying this phenomenon have a basis for comparison when discussing their work. The measure of elasticity of a collision is referred to as the Coefficient of Restitution (CoR), which varies from 0 (perfectly inelastic) to 1 (perfectly elastic). CoR is a common metric for characterizing collisions in particle-tracked CFD models. For experiments and models in internal cooling geometries, mass flow reduction and blockage per gram are often used metrics. Mass flow reduction is a measure of how mass flow is reduced at a constant pressure drop by the presence of a deposit narrowing the coolant passage. When normalized by the amount of dust delivered, it is called blockage per gram. Another metric when looking at deposits is

packing factor. Packing factor is the ratio of the actual density of a deposit to the theoretical 100% density of the deposit. In other words, it is a measure of porosity of a deposit. Less dense deposits might grow in height quicker and erode easier than more dense deposits, and there is evidence packing factor affects thermal conductivity of a deposit [12].

In both internal and external flows, another important metric is called capture efficiency, which will be referred to extensively in this work. Imagine dust-laden air traveling through a gas turbine engine. Some of the dust will travel straight through the engine without ever coming into physical contact with a solid surface. The fraction of dust entering the engine that does impact internal surfaces is given by the impact efficiency. See Equation 1. Even if the dust does impact a surface, it is not guaranteed to stick. As discussed above, some particles have a large enough rebound kinetic energy to not deposit on a surface. The mass fraction of impacting dust particles that do end up depositing is given by the sticking efficiency. See Equation 2. The capture efficiency then is the fraction of dust which enters the engine and not only impacts a surface, but deposits on it. Capture efficiency is shown in Equation 3; it can be calculated by multiplying the impact efficiency by the sticking efficiency.

$$Impact\ Efficiency = \frac{Amount\ of\ dust\ entering\ an\ engine\ which\ impacts\ a\ surface\ (g)}{Total\ amount\ of\ dust\ entering\ an\ engine\ (g)} \quad (1)$$

$$Sticking\ Efficiency = \frac{Amount\ of\ dust\ impacting\ a\ surface\ which\ deposits\ (g)}{Amount\ of\ dust\ entering\ an\ engine\ which\ impacts\ a\ surface\ (g)} \quad (2)$$

$$Capture\ Efficiency = Impact\ Efficiency\ x\ Sticking\ Efficiency \quad (3)$$

Chapter 3. Scope of Work

This study is primarily concerned with unpacking and understanding the effect of variable mineral chemistry on deposition in an impingement coolant jet. An 894K, round coolant jet with Re ~ 3800 exits a 6.35mm diameter-tube at flow velocity 57m/s and impinges on a backside-heated Hastelloy X target plate positioned 12.70mm (two exit diameters) downstream. Dust blends of various heterogeneous mineral content and 0-10μm particle size range are aerosolized and injected into the flow. In most cases, a deposit forms on the plate surface. Deposits are characterized by capture efficiency, deposit morphology, and X-ray diffraction analysis. Capture efficiency has already been introduced and the latter two will be discussed in more detail later.

AFRL02 was chosen as the control of the experiment. Employing the same substitution used by Crowe and Bons, in the absence of readily available aplite, albite ($NaAlSi_3O_8$), a type of alkali feldspar, was used instead [13]. Deposition experiments were conducted with each single mineral first, in order to understand how each mineral deposited in the absence of other mineral species. Then, AFRL02 was tested. The question was asked: "Does understanding of the behavior of the deposition of single minerals explain the mass, morphology, and chemistry of an AFRL02 deposit?" Next, quartz having been identified as a mineral of interest in deposition, dual-mineral tests (quartz with one other mineral) were performed both in simultaneous and sequential

format. Simultaneous dual mineral tests used blends of quartz with a second mineral in the same relative proportion between them as found in AFRL02. Sequential dual mineral tests began with delivering a half gram of a non-quartz, single mineral over four minutes. After just a few seconds of buffer time, a half gram of quartz was delivered over the remaining four minutes, impinging on the existing deposit. Finally, six "blends" were tested. Five of the blends each contained four out of the five minerals in AFRL02. Stated differently, in each of these five blends, one of the five minerals was *removed* from ARFL02, leaving the remaining four minerals in the same relative proportion found in AFRL02. By designing blends in this way, the contribution of each individual mineral on the net AFRL02 deposit was teased out. In the sixth blend, instead of subtracting a mineral, a small amount of hematite (Fe_2O_3) was added to AFRL02. Framed in terms of gas turbine engines, this hematite represents rust that originates in an upstream section of the engine and mixes with AFRL02 as it travels downstream. The blends used in this study are summarized in Table 3. The goals were to determine which minerals were most important in deposition, if synergies or reactions occurred between minerals in a blend, and what, if any, generalizations could be drawn to allow knowledge of AFRL02 to be applied to any arbitrary dust encountered in nature.

Table 3: Dust blends used in this study

Dust Blend Name	% Quartz	% Gypsum	% Albite	% Dolomite	% Halite	% Hematite
AFRL02	34%	30	17	14	5	0
Blend 1	0	45.5	25.8	21.2	7.5	0
Blend 2	48.6	0	24.3	20.0	7.1	0
Blend 3	41.0	36.1	0	16.9	6.0	0
Blend 4	39.5	34.9	19.8	0	5.8	0
Blend 5	35.8	31.6	17.9	14.7	0	0
Blend 6	32.0	28.4	16.0	13.2	4.7	5.7
Simultaneous Dual Mineral Test Blend Name	% Quartz	% Gypsum	% Albite	% Dolomite	% Halite	% Hematite
Blend 7	53.1	46.9	0	0	0	0
Blend 8	66.3	0	33.7	0	0	0
Blend 9	70.1	0	0	29.9	0	0
Blend 10	86.9	0	0	0	13.1	0
Blend 11	84.4	0	0	0	0	15.6

Internal temperatures of gas turbine engines vary with operating conditions and location inside the engine. The second goal of this study was to analyze the effects of plate surface temperature on deposition of different minerals and blends. It has previously been shown that capture efficiency generally increases with increasing surface temperature [14]. But the role of varied mineral chemistry on this trend is not clear i.e., whether or not capture efficiencies of different blends all follow the same temperature trend. Therefore, deposition was studied for single minerals and blends at three different plate front surface temperatures relevant to gas turbine engines: 1033K, 1144K, and 1255K. (Dual mineral tests, which were only performed at 1144K plate surface temperature, being exceptions.)

Outside the test campaign just outlined, two “supplemental” test series were run. An additional single mineral, alumina, was tested at just 1144K plate surface temperature. And an altogether separate dust blend, ARD, which was purchased from PTI, was tested at both varying plate temperature and varying flow temperature. Both Alumina and ARD were purchased already in the 0-10µm, range, as reported by the vendors. Most likely, the technique of milling and verifying size range differed from the method used for other dusts in this thesis.

Chapter 4. Literature Review Part I: Variables Affecting Particle Deposition in Gas Turbine Engines

Multitudinous studies have been performed in the past to identify the important factors affecting deposition including flow and surface temperature, particle/flow velocity, particle size, particle shape, and pressure inside the engine. In this chapter, a small subset of results is summarized.

Effect of Temperature

Deposition has been shown to increase with both increasing flow and surface temperature. Plewacki et al. used the High Temperature Deposition Facility (HTDF) at The Ohio State University to study deposition of ARD on ceramic targets in a hot flow ranging from 1623K to 1823K. They found a clear increase in dust captured with increasing flow temperature [15]. Using the same facility, Clark et al. found a similar trend for ARD deposition on cooled TBC surfaces. Instead of varying the temperature of the flow, they left it at a constant 1873K and varied the temperature of the coolant flow cooling the TBC. Once again, there was a clear trend of increasing capture efficiency with increasing surface temperature [16]. Whitaker et al. found that both mass flow reduction and blockage per gram increased with surface temperature when studying the clogging of coolant holes by ARD in an impingement array whose surface temperature

ranged from 1193K to 1536K [14]. The material and geometry were completely different than those used by Plewacki and Clark and their teams, yet the trend continued. In this thesis, the deposition with increasing surface temperature trend will be shown to continue with AFRL02 in a coolant flow impinging on a Hastelloy-X surface.

Effect of Particle/Flow Velocity

Local velocities inside of a jet engine can range from 60m/s at the combustor inlet all the way to 500m/s at the turbine inlet [17]. If there is a relative velocity difference between a flow and a particle entrained in the flow, a drag force will be applied to the particle, until it is accelerated/decelerated to the same velocity – therefore the velocity of the particle and flow are highly coupled. The effect of velocity on deposition is usually viewed from two perspectives. One perspective is velocity's contribution to the Stokes number,

$$St = \frac{\rho_p d_p^2 u_p}{18\mu_\infty L} \tag{4}$$

where ρ_p is the particle's density, d_p is the particle's diameter, u_p is the particle's velocity, μ_∞ is the dynamic viscosity of the gas and L is some characteristic length scale. A larger Stokes number particle will be less likely to follow a streamline and more likely to ballistically collide with a surface if the flow suddenly changes direction to avoid a solid object, such as a turbine blade. Since the number of particles colliding with a

surface increases with increasing St, it makes sense that the number of particles that eventually stick will increase, too, given a constant sticking efficiency. Zhang et al. pointed out that a higher velocity flow given a constant dust concentration means that a larger total amount of particulate will enter an engine [18]. So higher velocity should increase capture efficiency. However, velocity's other effect is that particles with higher velocity are more energetic, and thus more likely to rebound with higher kinetic energy or even erode an existing deposit.

Zhang et al. found these two mechanisms to be competing in an experiment of molten wax depositing on an airfoil surface near the melting temperature of wax [18]. At low velocities, the first mechanism was dominant, and capture efficiency increased with increasing velocity. However, at a critical velocity, the capture efficiency began decreasing, as the deposit was sheared off. Interestingly, not only did the capture efficiency change, but the deposit morphology did as well: higher velocity deposits tended to be smoother with less surface roughness.

Bowen et al. studied the deposition of 0-5μm ARD in an 811K impingement coolant jet. As they increased the jet velocity from 65 to 125m/s they found a nonlinear but monotonic decrease in both capture efficiency and cone size [19], placing these results in the kinetic energy-dominant region of Zhang's theory.

Singh and Tafti proposed a critical viscosity model for deposition, which takes into account both velocity and temperature effects in conjunction. They varied jet temperature from 1223K to 1323K for 20-40μm sand particles and plotted CoR vs. velocity. They found that large particles will rebound even at the lowest velocities, but

small particles conversely will stick with a 100% sticking efficiency until a critical velocity is reached, after which their CoR will increase slowly. At velocities over 40m/s they predicted minor differences in CoR based on particle size [20].

Effect of Particle Size

Particle size is another important variable in the Stokes number definition given by Eq. 4 above. More massive particles have more inertia, which prevents them from following a streamline smoothly. However, larger particles have a smaller surface area-to-volume ratios, meaning that two dimensional surfaces forces that promote sticking may not be as dominant over inertial forces as they are for smaller particles. Several studies have been performed to identify particle size's role in deposition. Bodjo et al. performed CFD modeling of both ARD and AFRL02 dusts of various size ranges in full-scale engine models. They determined there is a key subrange of particle sizes that is most responsible for deposition [21]. Upon visual inspection of their data, this appears to be between 1-10µm. This corroborates the findings of Whitaker et al. who studied blockage in an impingement hole array with an 866K coolant flow. They tested four size ranges of ARD (0-5µm, 0-10µm, 0-20µm, and 5-10µm) and found capture efficiency to decrease in exactly that order when all other conditions were held constant. Through some clever analysis, they determined particles less than 3.5µm were most responsible for blockage [22]. On the other hand, particles above 5µm exhibited the ability to erode existing deposits. Yet another study which corroborates these results was Wolff et al. who studied similar size ranges of dust blocking holes in a flat plate with effusion cooling

geometry at 1.03 pressure ratio, 150° hole turn, 1116K plate temperature and 950K coolant temperature. The 0-3µm and 0-5µm size ranges blocked an order of magnitude more than 0-10µm, 5-10µm, and 10-20µm size ranges [23].

From the above studies, one can conclude that smaller particles are more dangerous to engines. However, this conclusion may be the most applicable to coolant flows, where the temperatures are below melting temperatures of the minerals in the dusts. Two studies (Crosby et al. [24] and Bonilla et al. [25]) performed on an accelerated deposition facility at temperatures considerably higher than the aforementioned studies (1450K and 1350K, respectively) and a variety of other geometry and material variables (45°, TBC surface for Crosby, and CFM56-5B aero engine nozzle guide vane for Bonilla) showed a monotonic increase with particle size even at 20µm. This is attributed to the melting point of minerals being surpassed – even a large particle with high inertia will collide inelastically if molten.

Effect of Particle Shape

Little research has been done on the effect of particle shape on deposition, partially due to the difficulty of characterizing the multitudes of irregular shapes at the micron size scale [12]. Many computer simulations model particles as spheres, which simplifies modeling of particle trajectories in a flow, but leads to complicated impact and rebound physics [20, 17]. By modeling particles as cylinders with spring-like rebounds, the OSU deposition model solves the collision physics exactly [26].

One universally accepted reason shape is important is because it changes the drag characteristics of a particle. Drag regimes are separated into Stokes (low Re) and Newton (high Re) regimes. Connolly characterized Corey Shape Factors of ARD particles in both regimes using interferometry experiments [27]. Bowen focused on only the Stokes regime and determined a particle shape factor using Haider and Levenspiel correlations [28]. However, regardless of which regime and which metric used to characterize the particle shapes, an irregular shape (non-spherical) always acts to raise the drag coefficient. The more the shape deviates from spherical, the greater the change in drag coefficient, up to several orders of magnitude higher. Higher drag means the particle is more likely to follow a streamline through an engine, reducing the likelihood of a collision with an internal surface.

Two more potential areas where shape plays a role is in mechanical interlocking forces between particles [29], which could not happen between spheres, and erosion due to highly angular particles chiseling away at a deposit.

Effect of Pressure

Bowen and Bons suggested three mechanisms by which increased pressure affects deposition in an effusion cooling plate: 1) increase in effusion hole discharge coefficient, 2) altered particle trajectories due to reduced effective Stokes numbers, and 3) altered erosion of deposits due to reduced effective Stokes number [30]. They found marked changes (decreases) in mass flow reduction and blockage per gram as pressure was increased from 0.0001 to 0.0016 GPa in the High Pressure Deposition Facility (HPDF) at

The Ohio State University. Sacco et al. found that capture efficiency and peak deposit height decreased for the same range of pressures for deposition in an impingement cooling plate [31]. Lundgreen conducted a CFD study on internal cooling passages for much higher pressures: 0.1, 1, and 3 GPa. At these pressures and 1.015 and 1.03 pressure ratios, his model predicted an *increase* in capture efficiency with discharge pressure [32].

Chapter 5. Literature Review Part II: Chemistry's Effect on Deposition

The previous discussion of factors affecting particle deposition has led to several advances in understanding the phenomenon from a physics point-of-view. Several attempts have also been made to incorporate the effect of chemistry on the deposition problem.

Crowe and Bons explored the effects of dust chemical composition on deposition in effusion cooling geometries [13]. They observed that the effusion hole blockage rate of a mixture was not accurately predicted by a mass-weighted average of the blockage rate of each of the minerals contained within the mixture. In an attempt to explain their results, they looked at whether or not their data correlated with trends of the coefficients of restitution, Hamaker constants, dielectric constants, and melting temperatures of each mineral. Ultimately, they found no satisfactory correlation.

Song et al. also explored the effect of varying mineral chemistry on inter-particle fusion behavior of nine volcanic ash samples collected from around the world [33]. They concluded that knowledge of a set of four transitional temperatures associated with shrinkage, deformation, melting, and ultimately flowing, obtained through static heating tests, was enough to predict each sample's disposition for deposition. They next related these transitional temperatures back to chemistry through use of a simple metric: the ratio of basic to acidic oxides present in an ash sample. This is a valid approach, as at

temperature ranges relevant to gas turbine engines, within a CMAS deposit, the acidic oxides, SiO_2 and Al_2O_3, act as network formers, creating long aluminosilicate chains, whereas the basic oxides CaO and MgO interstitially diffuse into the aluminosilicate structure, and act as network modifiers, decreasing the number of oxygen bridges throughout the structure, which in turn decreases transition temperatures since there are fewer bonds to relax [34]. This is also consistent with conclusions from Dunn's landmark study of full-scale engine deposition tests. He demonstrated that the relative proportion of Ca (basic) to Si (acidic) in a dust mixture is an important metric to predict deposition [35]. Poerschke et al. also concluded the ratio of Ca to Si was the best metric to predict liquid infiltration of TBCs for experiments run at 1573K [36]. However, the *absolute* accuracy of metrics like these used in fields outside of gas turbine engines, such as agglomeration in fluidized bed combustion, has been called into question [37].

What Song, Dunn, Poershke and their teams noticed were the effects of minerals in solid solutions forming alkali/alkaline-earth aluminosilicate eutectic systems. These eutectic systems have properties very different from their individual constituents, e.g., transitional temperatures.

Chapter 6. Literature Review Part III: Introduction to Fluidized Bed Combustion and Its Contribution to Knowledge of Mineral Eutectics

A large portion of this thesis' discussions on chemistry benefitted from research being performed in the field of agglomeration in Fluidized Bed Combustion (FBC). In FBC, a bed material, usually silica, composed of ~1mm particles, is "fluidized" by blowing air through it above a critical pressure drop [38]. Biomass ash of particle size 30-600μm is added and combusted to heat steam, which is used for power generation. Much attention has been paid to this field recently because it is efficient and much more carbon-neutral than burning fossil fuels. A standard operating temperature range in the combustion chamber is 943-1143K [37]. As the organic matter combusts, particle sizes shrink, and can reach the 1-10μm range [39]. At this size range, mainly noncombustible, inorganic molecules are left. These can include quartz, gypsum, albite, dolomite, halite, and hematite [40, 41]. Like in gas turbine engines, mineral content is heterogeneous and varies widely by source. Inside of the combustor, these minerals react with the quartz bed material to create low-melting point eutectics which stick to each other via random collisions and form agglomerations. These agglomerations can lead to "defluidizing" of the bed material, upon which the whole process comes to a screeching halt and the plant must be shut down for cleaning. The agglomeration phenomenon has been costly enough to spur a huge amount of research into understanding its causes and prevention. Despite fundamental differences between agglomeration in FBC and deposition in gas turbine

engines (notably the sizes of the particles, the velocities of the particles and flow, the addition of organic debris, etc.), much of the underlying chemistry is the same.

Various reviewers agree that the most important chemistry driving agglomeration in FBC is the formation of alkali silicate eutectics [12, 37, 40, 41]. The reason being that eutectics have markedly lower melting temperatures than their constituents. An agglomeration which is softened or melted will absorb more kinetic energy from incoming particles leading to more inelastic collisions. Lower transitional temperatures also lead to lower viscosity and surface tensions of agglomerations. In silicate-rich ashes, viscosity and surface tension are perhaps the most important metrics to predict particle stickiness. Whereas, in salt-rich ashes, melt fraction is more important [12]. Regardless, all of these can be directly related back to chemistry.

When comparing alkali/alkaline-earth silicates, Morris found that potassium-containing melts had lower melting temperatures than sodium-, magnesium-, or calcium-containing melts [37]. And that the more silica was added to the melt, the lower the melting temperature was. For example, in the general formula $K_2O \cdot nSiO_2$, when n = 1, the melting temperature is 1249K. This decreases with increasing n; when n = 4, the melting temperature is 1037K [37]. Potassium- and sodium-containing silicate melts are potentially more dangerous to jump starting deposition because of the formation of these low-melting temperature eutectics. However, if magnesium and calcium are available, they will substitutionally diffuse into the melt, replacing the sodium and potassium. The sodium and potassium are volatilized off as gasses. (These gasses then go on to reap destruction in other parts of the engine. They can recombine with, for example, a gaseous

SO_3 ion to form alkali sulphates that can cause sulfur erosion.) Magnesium- and calcium-containing melts inherently have higher melting temperatures than alkali-containing melts, and these higher-melting temperature crystals will precipitate out and harden on as CMAS deposits. Morris also looked at some agglomeration formation time trends with other variables. The most major and notable trends were an increase in agglomeration with increasing temperature, a decrease in agglomeration with increasing velocity, and an increase in agglomeration with increasing particle size. There have been verified counter examples to this last trend with particle size. All three trends sound very familiar to trends in deposition in gas turbine engines outlined above.

Kleinhans et al. and Vassilev et al. also emphasized the importance of incorporation of variables outside of chemistry. Vassilev et al. pointed out that bulk chemical composition (such as how researchers in gas turbine engines often only report ARD's total oxide content) is important, but the exact minerals and phases must also be known to fully understand the agglomeration process [40]. That point will become one of the greatest conclusions of this thesis for deposits in an impingement coolant jet at conditions relevant to gas turbine engines. According to Kleinhans et al., one major mechanism that affects final capture efficiency of a deposit is erosion of an existing deposit. There are three mechanisms listed in the literature for erosion of a deposition off a coal combustor's wall: 1) shedding due to mechanical stresses; 2) erosion caused by sharp, nonmolten particles colliding with an existing deposit; and 3) dripping of low-viscosity deposits off a surface [12]. Kleinhans et al. also report that pressure inside of the combustor can affect the condensation of alkali gasses, such as those outgassed

during calcium-substitution outlined above, and that whether the atmosphere is oxidizing or reducing is important to agglomeration: a reducing atmosphere can often lead to fusion temperatures that are 50K lower than the same eutectic melt in an oxidizing atmosphere [12]. The hot section of a gas turbine engine is usually exposed to an oxidizing atmosphere, but local and temporary reducing atmospheres can be created, especially during takeoff [42].

Chapter 7. Literature Review Part IV: Impingement Flows

The hot section (combustor and high-pressure turbine) of a gas turbine engine consistently operates at temperatures which exceed the melting temperatures of the materials which it is constructed from. This would make operation of a gas turbine engine impossible if not for the coolant architectures implemented to keep temperatures down. One of the most common cooling architectures in the hot section, and the focus of the present study, is impingement cooling. The literature review ends with some background on these types of flows and their uses in gas turbine engines.

Flow Field

It is generally agreed that an impingement jet transitions from laminar to turbulent around Re of 3000 [43, 44]. The flow field of a round jet impinging on a flat plate can be separated into three regions: 1) a free jet region; 2) a stagnation flow region; and 3) a wall jet region. A schematic of the three zones is given in Figure 6. The free jet region develops upon expulsion from the exit hole, where upstream effects from the plate's presence are negligible. As the fluid travels downstream in the free jet region, shear effects between the jet's boundary and surrounding, ambient air diffuse inwards. This creates a potential core – a region where there is no influence from shear – which persists four to six diameters downstream [43]. The stagnation flow region by contrast is highly

affected by the presence of the plate. All of the velocity normal to the plate's surface must go to zero at the boundary of the plate surface and the flow is forced to turn outwards. This creates a stagnation point with high pressure directly in the center of the flow field. Particles entrained in the flow, especially larger particles with higher Stokes numbers will be unable to change direction as quickly as the air molecules and we would expect a high impact efficiency in this area. The final region is the wall jet region. Once the flow has turned 90 degrees, a boundary layer develops along the wall traveling outwards. The magnitude of shear force decreases radially in the wall jet region.

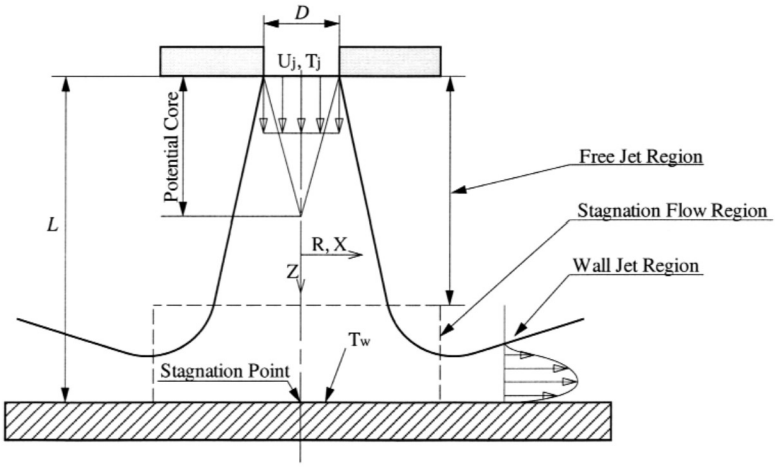

Figure 7: Flow field for round jet impinging upon a flat plate [43]

Heat Transfer

In this experiment as well as inside of jet engines and many other convective heat transfer applications, impingement flows are utilized because of their ability to convectively cool the metal surface – convective heat transfer for impingement flows is up to three times greater than that for a basic parallel wall flow [44]. Despite a simple-looking geometry, the heat transfer process is complex and depends on the distance between the hole's exit and the plate surface (normalized by diameter, H/D), radial distance (r/D), Re (more turbulent flows have higher degree of heat transfer), Mach number, pitch between jets (when multiple jets present), and area [44]. It is standard to characterize the heat transfer according to the Nusselt number,

$$Nu = \frac{hD}{k} \tag{5}$$

where the heat transfer coefficient, h, depends on the temperature of both the fluid and wall, D is the diameter of the jet, and k is the thermal conductivity of the fluid [43].

Impingement Arrays in Gas Turbine Engines

In gas turbine engines, the cool air used in the impingement flows is bled off from the compressor [44]. There are several important differences between impingement cooling in this experiment and that in real jet engines. The first is the size of the impingement jet. The second is the geometry. In this experiment a long, single tube is

used, whereas in a real jet engine there would be an array of drilled holes, which would have a very different pressure drop when compared to a long pipe [44]. This array would create interactions between jets, such as fountain regions between jets where air would lift off the plate surface and can also affect heat transfer [43, 44]. Typical Re are 4000 to 800,000 and typical H/D are 2 to 12 [44]. In this thesis, Re is 3800 and H/D is 2, at the low side of both spectra.

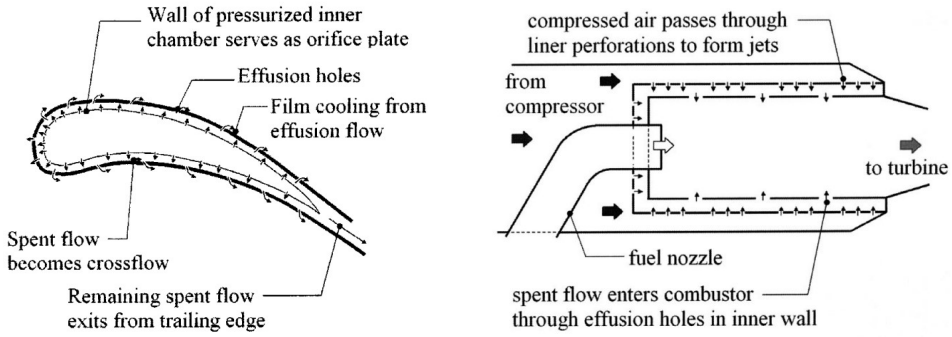

Figure 8: Employment of impingement cooling in turbine blades and combustor liners of gas turbine engines [44]

Chapter 8. Experimental Set-up and Procedure

Summary of Experiment

For each eight-minute experiment, nominally one gram of aerosolized, 0-10μm mineral dust was fed at a constant rate into a 3.66m long, 6.35mm inner diameter tube, whose internal flow was driven by mass flow controllers. Inside the tube, the two-phase flow was heated to 894K, and accelerated to 57m/s, as measured at the exit of the tube. After exiting the tube, the air-dust mixture impinged normally upon the center of a Hastelloy X plate, positioned 12.70mm (two tube diameters) downstream of the exit. The plate was heated from behind with a methane-oxygen torch at the same time as it was cooled from the front by the impingement flow. Balanced between the heat fluxes of the torch and the flow, a steady-state surface temperature (1033K, 1144K, or 1255K, depending on the experiment) on the front (cooled side) and center of the plate was verified prior to dust delivery. Other testing conditions, summarized in Table 4, remained constant for all tests. In most cases, a mineral dust deposit formed on the plate surface during delivery. Each experiment was repeated three times.

Table 4: Test conditions

Condition	Value
Impingement Jet Flow Speed	56.9 +/- 0.3m/s
Impingement Jet Flow Temperature	894 +/- 4K
Tube Diameter	6.35mm
Distance Between Tube Exit and Plate	12.70 +/- 0.50mm
Impingement Angle	90 +/- 1°
Plate Temperature Uncertainty	+/- 8K
Dust Delivery Rate	1g / 8min
Particle Diameter Distribution	0-10µm
Uncertainty in Capture Efficiency	+/- 0.008

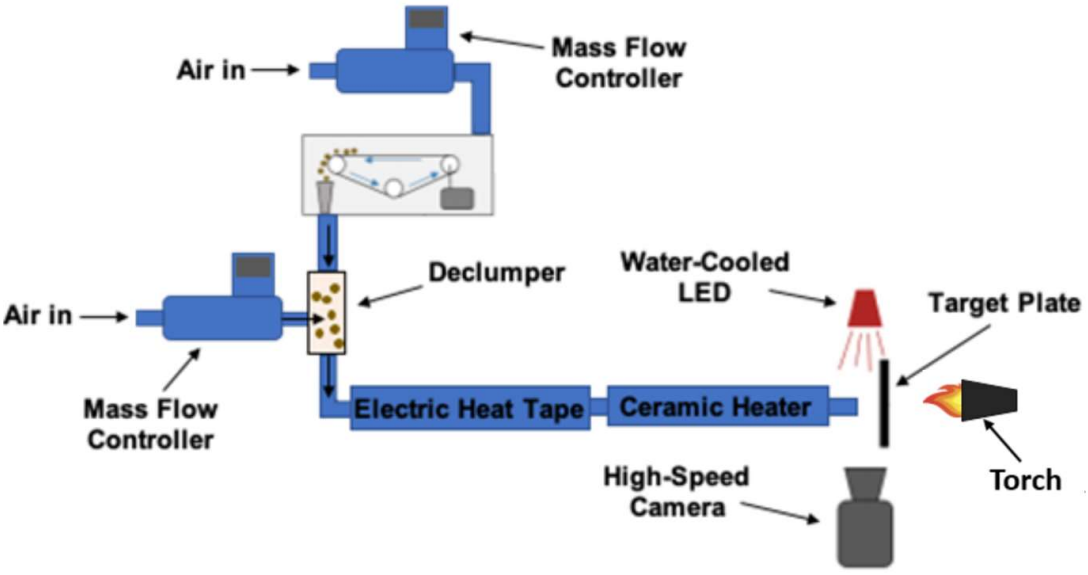

Figure 9: Impingement Deposition Rig

Figure 9 shows a schematic of the Impingement Deposition Rig. Before each experiment begins, approximately one gram of dust is weighed on a scale with 0.0001g accuracy and spread with a scoopula evenly onto a conveyor belt, which is housed in a

pressurized feed box. The box is then clamped shut – rubber gasket material ensures the box remains airtight. The pressure in the box, which drives the flow down a funnel and into the tube ("main line"), is supplied by a mass flow controller. The mass flow necessary to reach the 57m/s exit velocity is 35.9SLPM. Of this, 18.9SLPM is supplied to the feed box. After dropping off the conveyor belt through the funnel, but before reaching the main line, the dust passes through a deagglomerating device. The remaining 17SLPM is supplied by a second mass flow controller to the deagglomerating device (discussed in more detail below), which aerosolizes the dust. To heat the flow, a series of three eight-foot electric-resistance heater tapes is wrapped around the length of the main line. A ceramic inline heater is used instead for the final 0.46m. The temperature of the flow is measured by suspending a K-type thermocouple bead directly in the center of the exit flow. For known mass flow, cross-sectional area of the main line, and temperature-dependent air density, the exit velocity can be calculated from the mass flow rate equation:

$$\dot{m} = \rho A v \tag{6}$$

The 76.2mm x 76.2mm x 3.17mm-thick target plate and torch used for heating the plate are both mounted upon a translationally- and rotationally-adjustable carriage. The plate temperature is verified via a plate with a K-type thermocouple embedded in its surface. The plate material is Hastelloy X, a nickel superalloy comprised of nickel (47%),

chromium (22%), iron (18%), molybdenum (9%), as well as other trace elements. A new plate is used for each experiment.

The Declumper

One of the greatest challenges of working with fine, particulate dusts in the laboratory is overcoming room-temperature agglomeration. Agglomeration is the spontaneous formation of large, loosely packed agglomerates from a collection of smaller particles due to liquid bridges (water) between particles, van der Waals forces, electrostatic forces, solid bridges, mechanical interlocking, or combinations of the above mechanisms [29]. Agglomerates' deposition behavior has been shown to be different than deposition of a fully aerosolized dust, creating larger, more compact deposits [45]. Overcoming these forces to break up agglomerates is not trivial, especially when working under mass flow and geometry constraints. For this experiment, a deagglomerating device (hereafter referred to colloquially as "the declumper") was utilized. The declumper employs its own mass flow controller to create a confined, high-velocity, high-shear, flat jet of air, which the dust encounters as it drops from the feed box into the main line. A high-shear jet can create inertial stresses, shear stresses, and turbulent stresses – all of these have been shown capable of breaking up agglomerates [29]. Shadow Imaging results revealed the declumper succeeded in breaking up about 90% by volume of dust leaving the main line to sizes below the detectable limit, or less than 15μm. This deagglomeration step is very important because dust in the atmosphere,

which we are attempting to model, is usually found aerosolized as opposed to in agglomerates.

Dust Milling and Sizing

Particle size has a first-order effect on deposition of mineral dust on surfaces [23]. For this study, a dust particle diameter distribution of 0-10μm was desired. It has been confirmed that dust ingested into a gas turbine inlet is efficiently pulverized by the compressor blades into nominally this size range [35]. This is also the most important subrange of particle sizes affecting deposition [21]. The mineral dusts were milled in-house to the 0-10μm range. To verify the size ranges, about 18,000-24,000 particles per mineral were photographed under a 50x microscope and analyzed with the particle- and grain-sizing software, MIPAR^{TM}. The cumulative volume percent statistics from this analysis are graphed in Figure 2.

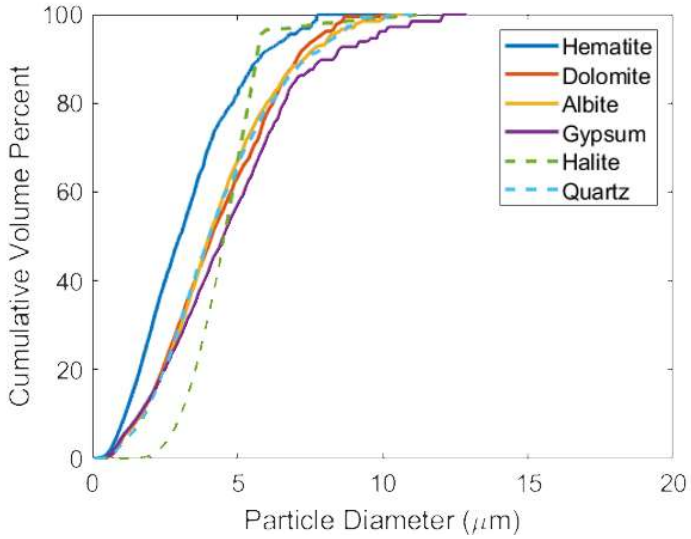

Figure 10: Cumulative volume statistics for mineral dusts used in this study

Chapter 9. Methods of Data Collection and Analysis

Capture Efficiency

Capture efficiency was introduced in Chapter 2. Capture efficiency is the ratio of the mass of the deposit to the mass of dust that exited the main line to be delivered to the plate. The mass of the deposit was measured by subtracting the mass of the plate prior to the experiment from the mass of the plate with deposit after the experiment. The mass of dust that exited the tube was calculated by subtracting the mass of dust losses, such as dust which stuck to the inside of the main line during the test and was cleaned out after the test, from the dust originally loaded on the conveyor belt. The dust was cleaned by using particle-trapping air filter material and wiping down any surfaces, such as the belt and funnel, that had residual dust. The dust within the tube was cleaned out by securing multiple layers of filter on a makeshift "end cap," that capped the end of the main line and prevented air escaping except through the filter portion. Then, 34.4kPa of air was blown through the tube for a period of about 3-5 minutes and the mass change of the filter was recorded. Typically, 1.4g of dust were loaded on the conveyor belt per test, and 0.4g of dust was lost within the system and did not exit the main line. Despite best efforts to clean out all residual dust, it is estimated a maximum of 0.08g of dust per test went unaccounted for. From this, a +/- 0.008 uncertainty in all reported capture efficiency values was calculated.

X-Ray Diffraction

Powder X-ray diffraction (XRD) was performed on pulverized deposits with a Rigaku MiniFlex 600 at the Center for Electron Microscopy and Analysis at The Ohio State University. Data was analyzed with PDXLII software. The fundamental assumption of XRD is that the heterogeneous mixture of crystals which make up a sample are randomly distributed with an even distribution of orientations. An X-ray source is shone onto the surface of a sample at angle, θ. The X-ray penetrates some distance, δ, into the bulk of the sample, which is greater than the interatomic spacing, d. Parallel X-rays rebound from the sample to a detector, also at angle θ. These X-rays will interfere with each other forming a diffraction pattern. From this diffraction pattern, an interatomic spacing, d, can be determined, which will be unique to every bond (e.g., a Na-Cl bond will have a different bond length than a Si-O bond). The spacing, d, is determined by Bragg's Law. A schematic of Bragg's Law is given in Figure 11. PDXLII compares an experimentally-obtained spectra with over 19,000 database entries of known substances and calculates potential matches via the Relative Intensity Ratio (RIR) method. An uncertainty is subsequently quantified as a Figure of Merit (FOM). The major drawback of XRD as a method for detecting mineral composition of a deposit is its inability to detect amorphous phases, which do not have well-defined bond lengths. This is especially adverse to understanding the chemistry of glassy deposits formed on the 1255K plate, where most likely a high amount of amorphous phases were still present after cooling.

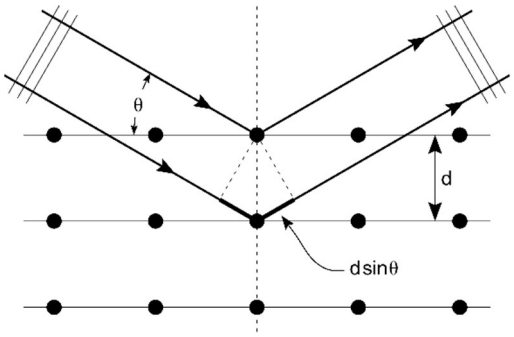

Figure 11: Bragg's Law, governing principle of XRD [46]

The goal of XRD was twofold: to understand if any chemical reactions were occurring either between two or more minerals, or between minerals and the plate; and to determine if all minerals in ARFL02 or other blends deposited according to their single mineral capture efficiencies. The results have been reported as mass percentages, i.e., the results always add up to 100%, regardless of the mass of the deposit. When viewing XRD results, the reader is urged to keep in mind the relative sizes of deposits, as indicated by capture efficiency results, differ between samples.

XRD was not repeated for each repeat test. For experiments at 1033K plate surface temperature, the deposits were often so small that all three repeat tests had to be combined into one XRD sample. For experiments at 1144K plate temperature, it was not necessary to combine samples, but it was also not deemed necessary to run XRD on every test. Finally, for some experiments run at 1255K plate temperature, where there was an obvious distinction between the central deposit and outside region, the two regions were isolated and analyzed separately, to determine if certain minerals were more prone to depositing in certain regions of the plate. It was also not deemed necessary to

run XRD on single mineral tests, except in the case of dolomite at 1255K plate surface temperature, as discussed below.

Deposit Morphology

After each test, the plate was unmounted from the rig, and pictures were taken of the deposit plumb to the plate surface. Whereas capture efficiency was a purely quantitative measurement, deposit morphology analysis was qualitative in nature. As such, it would be useful to introduce some of the terminology used to describe deposit morphology now.

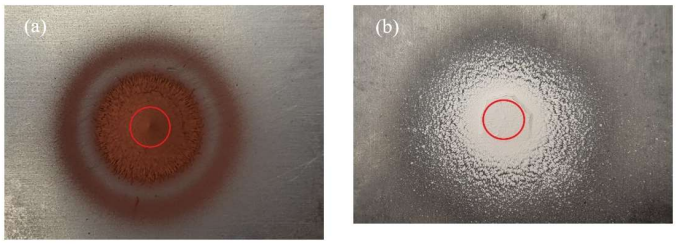

Figure 12: Deposits formed at 1144K surface temperature (a) hematite (b) AFRL02

Figure 12a is a picture of a pure hematite deposit on a plate which was heated to 1144K. Figure 12b is a picture of an AFRL02 deposit on a plate which was heated to 1144K. Together, these examples represent two common, yet distinct types of morphologies seen in experiments of this thesis. In both pictures, a red circle has been added. According to the scale of each picture, the circles have a 6.35mm diameter – which is the same as the

inner diameter of the main line. The red circles also indicate the approximate position of the main line exit relative to the deposit.

Describing the hematite deposit radially outwards, it has a large, conical "central deposit" (quotations denote the author's terminology), a "gap region" with very little to no deposition, and an outer, ringlike "halo region" where a small amount of deposition resumes. On the other hand, the AFRL02 deposit has a flattened central deposit. (One can also see just outside the red circle in Figure 12b that the central deposit has cracked upon cooling due to a difference in coefficients of thermal expansion between the deposit and plate. At even higher plate temperatures, it was not uncommon for the entire central deposit to sputter off the plate upon cooling.) In the AFRL02 deposit, a "speckled region," occupies the area outside of the central deposit in place of the gap and halo regions of the hematite deposit.

The above examples are not all-inclusive of morphologies presented in this paper, but describing other morphologies will be much easier with the terminology and context of the above examples.

Besides understanding the final morphology of a deposit, it is sometimes desired to understand the transient growth of a deposit. For this, a Shadow Imaging System is utilized. A red LED array is placed to one side of the plate, casting a side-profile shadow from the deposit, which is recorded by a Photron Fastcam SA-Z high-speed camera, situated on the other side (see Fig. 8). A Matlab script developed in-house detects the boundary of the deposit via binarization of black-and-white pixels. A deposit volume is estimated by, first, trapezoidally-integrating the two-dimensional profile, and then,

assuming cylindrical axisymmetry of the deposit, integrating again in three-dimensional cylindrical coordinates. In the present thesis, Shadow Imaging results will mainly be discussed for sequential dual mineral tests, but will be revisited in the Discussion section while elaborating on some observations about deposit formation.

Chapter 10. Results and Analysis

Single Mineral Dust Tests Results

The five mineral constituents of AFRL02 (quartz, gypsum, albite, dolomite, and halite) and hematite were deposited at 1033K, 1144K, and 1255K plate surface temperatures. Each test was repeated three times and the capture efficiency results were averaged. They are shown in Figure 13. Each bar is the average capture efficiency of three tests, and the error bars span the maximum and minimum values for the three tests. Results are graphed in order of descending capture efficiency, according to the 1144K case. Representative pictures of each mineral deposit at each temperature are shown in Figure 14. The red circles in the pictures represent the 6.35mm inner diameter main line from which the dust-laden air is exiting.

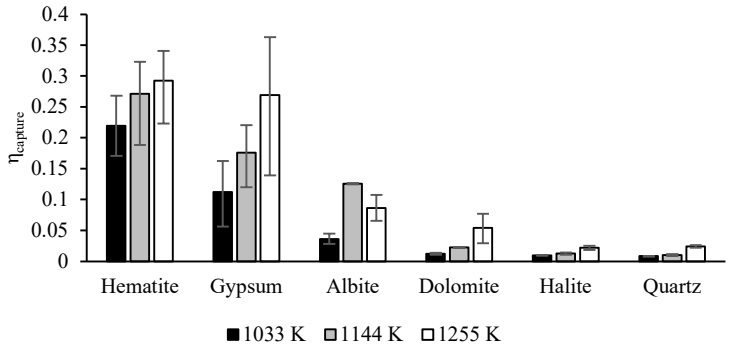

Figure 13: Capture efficiencies of single mineral dusts

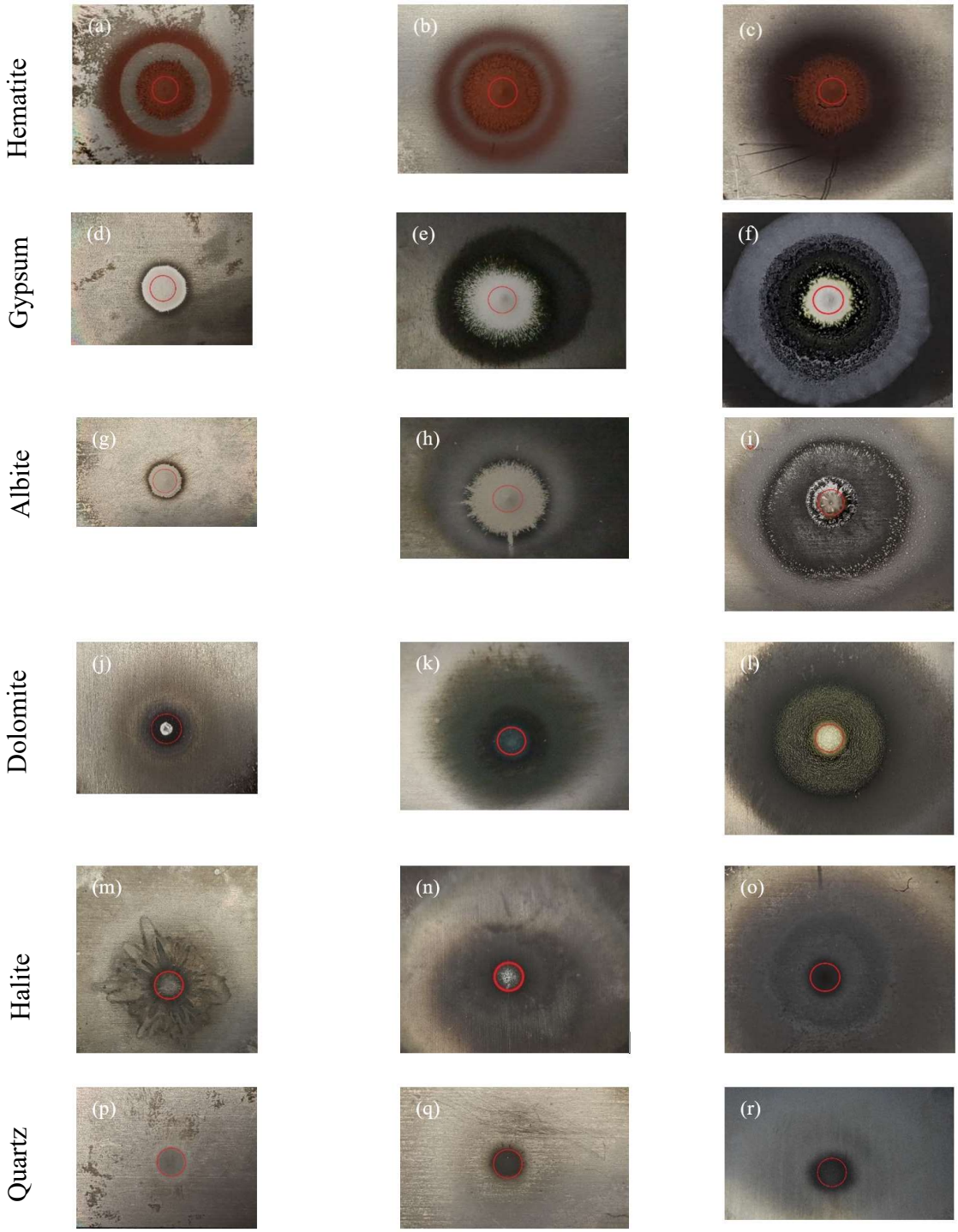

Figure 14: Representative pictures of each single mineral dust's deposits; Column 1 = 1033K, Column 2 = 1144K, Column 3 = 1255K

At all plate surface temperatures, hematite had the highest capture efficiency and gypsum had the second-highest capture efficiency. Albite, with the third-highest capture efficiency at all plate surface temperatures, was the only dust whose capture efficiency did not monotonically increase with temperature. As a deposit builds, it blocks the impingement flow, which is acting to cool the plate. This leads to overheating of the plate surface as the test progresses. It was observed that in the 1255K plate surface temperature case for albite, a transitional temperature of albite deposits must have been exceeded; the deposit became glassy and spread radially outwards in the face of the impingement flow. (Albite's glass transition temperature is 1038K [47] and its melting temperature is 1391K.) Some of this deposit material was lost off the edge of the plate. If this lost albite deposit could have been recovered and accounted for in the capture efficiency measurement, it would most likely recover the prevailing trend of monotonic increase with temperature. Dolomite, like gypsum, does not melt. They decompose into alkali/alkaline-earth oxides and volatile gasses. Also like gypsum, dolomite deposits turned green at higher temperatures, signifying a chemical reaction had occurred. But unlike gypsum, dolomite had a very low capture efficiency. Halite had the second lowest capture efficiency of all single minerals. Halite was the most difficult dust to deagglomerate, even with use of the declumper. Also, halite has a melting temperature of 1074K – below the conditions of two of our experiments. It was observed to liquify very quickly on the surface of the plate or, if delivered in large agglomerations, bounce off the plate and not deposit at all. At all temperatures, quartz deposited the least – its deposits were often barely perceptible. This is in contrast with Crowe and Bons who did find

quartz capable of blocking effusion cooling holes, albeit at a flow temperature 55K hotter.

It was generally unnecessary to perform XRD on single mineral deposits. However, at higher plate temperatures, both gypsum and dolomite caused the plate's surface – as well as part of the deposit itself – to turn green and/or black, signifying some sort of chemical reaction had taken place. XRD was performed on the dolomite deposit at 1255K plate surface temperature pictured in Figure 14. These results (Figure 15) suggest that the plate was, in fact, oxidizing. Cr_2O_3 is green and Fe_3O_4 is black, which agrees with visual observation of the deposit and plate color. It is surmised that during the decomposition of gypsum or dolomite, an oxidating atmosphere is present at the metal surface. Metal oxides diffuse into the deposit after their formation to cause the color change in the deposit.

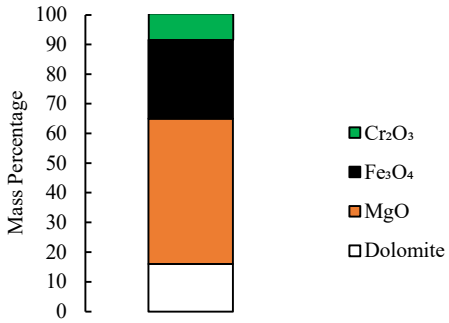

Figure 15: XRD result for dolomite deposit at 1255K plate temperature

AFRL02 Dust Tests Results

Now, deposition results of the experimental control, AFRL02, are reported. Figure 16 shows sample pictures of AFRL02 deposits at the three different plate temperatures. At 1033K, a very small and flat, central deposit exists. Outside of a gap region, there is also the slight shading of a sparse halo region. The 1144K case has the flat central deposit and speckled region, as discussed earlier. The picture of the 1255K plate temperature case is missing the white-colored, wafer-like central deposit, which sputtered off during cooling but was collected separately for capture efficiency measurements. There is the appearance of a gap region, which is actually a thin, glassy layer on the plate surface, and not a true gap in deposits. Then there are larger, speckled pieces of deposit in a halo region.

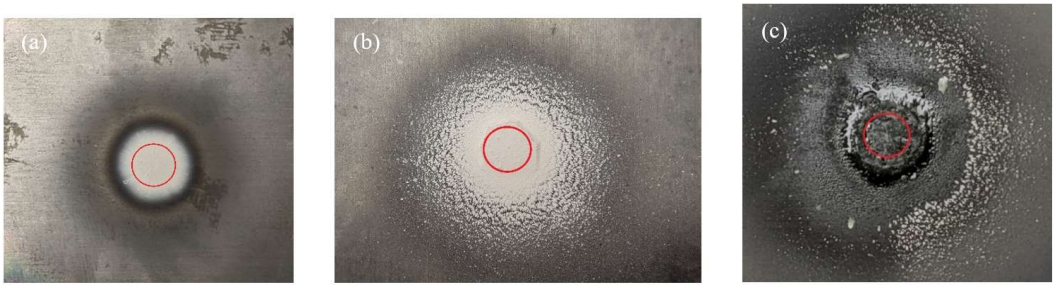

Figure 16: AFRL02 deposits at (a) 1033K (b) 1144K and (c) 1255K plate surface temperatures

The question could be asked can knowledge of the deposition behavior of single minerals be used to predict the deposition of AFRL02? In the case of morphology, the

answer is no. No single mineral produced morphologies of precisely the same appearance as those seen in the 1033K and 1144K plate surface temperature cases for AFRL02 (Fig. 16a&b). Although the 1255K case has similarities to albite's morphology (Fig. 14i), it would not have been expected for albite alone to determine the morphology, given a larger amount of the highly-depositing gypsum was also present in the mixture.

Next, a similar analysis is applied to capture efficiency results. A "hypothetical AFRL02" capture efficiency is calculated as a mass-weighted sum of the experimentally obtained capture efficiencies of each single mineral. In Figure 17, this hypothetical AFRL02 capture efficiency is plotted against capture efficiencies of the experimentally tested AFRL02 and of the single minerals. For the 1033K case, the hypothetical calculation overestimates the capture efficiency of experimental AFRL02 by a factor of three. However, there is good agreement for the 1144K and 1255K cases. This might lead one to believe that each mineral within the blend deposits independently of the other minerals, and it is therefore possible to predict the capture efficiency of any dust blend by knowing the capture efficiencies of its individual components. However, this conclusion rests upon the assumption that each mineral within a blend deposits independently. It will be shown this is *not* the case.

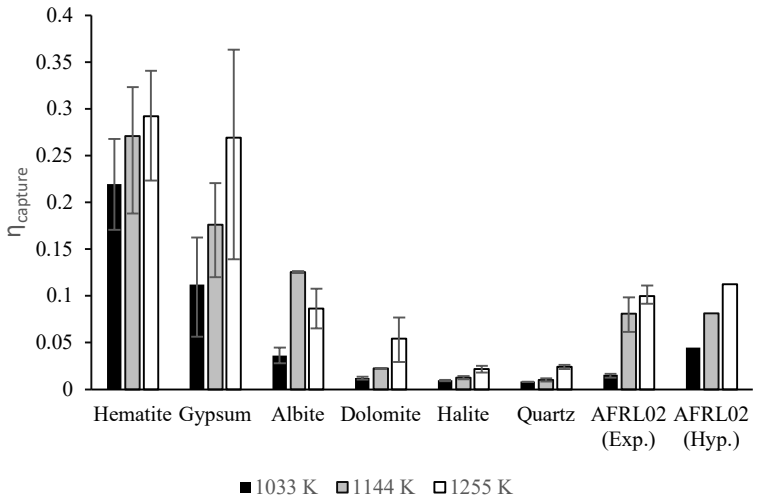

Figure 17: Capture efficiency results for experimental and hypothetical AFRL02 compared to single mineral capture efficiency results

To confirm or negate the validity of this assumption, XRD results for deposits at each of the plate temperatures are examined. Experimental AFRL02 versus hypothetical AFRL02 XRD results are shown in Figure 18. Hypothetical AFRL02 XRD results were calculated by multiplying the mass percentages of each mineral as it occurs in AFRL02 by the corresponding single mineral capture efficiency, from Fig. 13. For the 1255K case, central deposit (~two main line diameters) is analyzed separately from the specks in the halo region. Recall these data are reported as mass percentages and are not normalized according to total mass deposited.

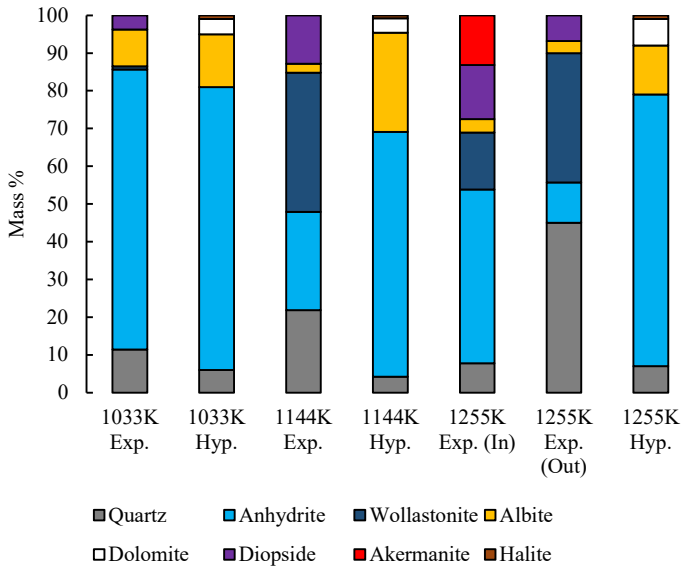

Figure 18: Experimental and hypothetical XRD results for AFRL02 deposits at three plate surface temperatures

A noteworthy observation from Fig. 18 is that new minerals were found in the AFRL02 deposit samples. Dolomite is never found in any deposit, but diopside ($CaMgSi_2O_6$), a product of dolomite and quartz, is found in every sample. Akermanite ($Ca_2MgSi_2O_7$) was potentially formed the same way, but as we will show later, could also be a product of dolomite and albite. Gypsum dehydrated into anhydrite ($CaSO_4$); and another common new mineral is wollastonite ($CaSiO_3$), which is a product of gypsum and quartz. A summary of the new minerals is given in Table 5.

Table 5: New minerals formed in AFRL02 deposits

Mineral	Chemical Formula	Melting Temperature (K)	Proposed mechanism of formation
Anhydrite	$CaSO_4$	Anhydrite decomposes into CaO and SO3 at 1473K	Dehydration of gypsum between 373K and 573K [40].
Wollastonite	$CaSiO_3$	1813	Reaction between gypsum and quartz [48]
Diopside	$CaMgSi_2O_6$	1665	Reaction between dolomite and quartz [48]
Akermanite	$Ca_2MgSi_2O_7$	1827	Reaction between dolomite and quartz or albite between 973K and 1573K [40]

From the experimentalist's perspective, one striking conclusion of this XRD analysis is the substantial amount of quartz, either in its pure form or as a product of a reaction, present in the deposits. At 1144K plate temperature, quartz, wollastonite, and diopside make up 71.6% of the total deposit. Not including the SiO_2 in albite, SiO_2 from these three sources comprises 48.1% of the deposit. This is significantly higher than the prediction of less than 10% quartz based solely on quartz' single mineral deposition behavior. There was also a high proportion of pure quartz – 40% – detected in the outer region of the deposit on the plate heated to 1255K.

If a heterogeneous dust mixture (like AFRL02) created a deposit whose capture efficiency could be accurately predicted using the capture efficiencies of each of its

mineral constituents, then the experimental and hypothetical XRD results above should match. They do not. Instead of a "hypothetical deposit" dominated by copious amounts of gypsum and albite, the experimental results confirm that quartz deposits more than expected and reacts with gypsum and dolomite to create new, low-melting temperature minerals. This finding is consistent with a recent study of engine deposits by Elms et al. who found that deposits had distinctly different mineral content than the minerals present in the dust that was injected into the engine inlet. Specifically, they found that their deposits included finite amounts of wollastonite and diopside [49].

Dual Mineral Dust Tests Results

Quartz is of special interest since it comprises the largest fraction of AFRL02. From a practical point of view, quartz is one of the most prevalent minerals found in the earth's crust the world over. Wood et al. identified it in 13 out of 13 diverse samples of dust and dirt from around the globe [9]. Quartz deposited the least of any single mineral, yet XRD results of the AFRL02 deposits showed that it deposited significantly in its pure form in the presence of other minerals. Quartz also reacted with dolomite and gypsum to form the single-chain silicates diopside and wollastonite, respectively. Given this motivation, it was desired to understand how quartz interacts with gypsum, albite, dolomite, halite, and hematite, separately. Thus, "dual mineral" tests were run at 1144K plate surface temperature.

Sequential Dual Mineral Dust Tests Result

Approximately a half gram of either gypsum, albite, dolomite, halite, or hematite was delivered to a 1144K plate to form a deposit, then a half gram of quartz was delivered on top of that deposit to determine the interaction of quartz with the existing deposit of the other mineral. Figure 19 is a composite cumulative volume plot obtained via the Shadow Imaging technique, as explained in Chapter 9. The dependent variable, time, has been normalized by the total test duration T; transition from the accompanying mineral to quartz occurred at roughly t/T equals 0.5.

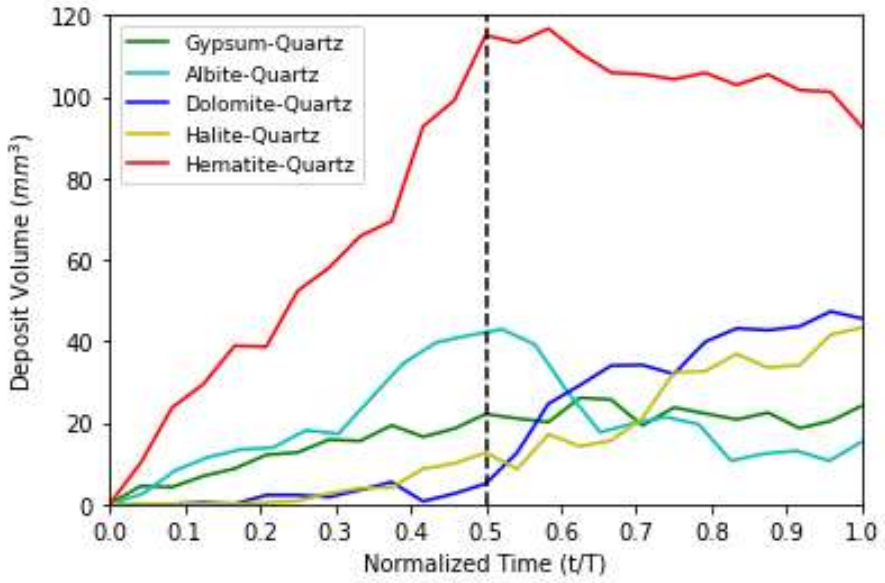

Figure 19: Cumulative volumes of sequential dual mineral deposits at 1144K plate surface temperature

Three distinct behaviors were observed. 1) Hematite and gypsum deposits both eroded very slowly as the effect of quartz bombardment. 2) Albite on the other hand was rapidly eroded by the quartz; albite lost half of its volume in just one minute of quartz impingement. 3) Both dolomite and halite, which barely deposited by themselves at this plate temperature, captured quartz. In fact, they captured enough quartz that the final volume of the deposits exceeded both those of gypsum-quartz and albite- quartz, gypsum and albite having deposited greatly as single minerals.

Simultaneous Dual Mineral Dust Tests Results

The sequential dual mineral tests led to important discoveries about the interaction between quartz and other minerals in AFRL02. Would the findings be similar in a test where quartz and the other minerals were delivered concurrently, in proportions dictated by AFRL02? For this, simultaneous dual mineral tests were conducted at 1144K plate temperature. Figure 20 shows capture efficiency results, with AFRL02 and quartz results added for comparison. Each test was repeated twice, except for blend 11, with hematite.

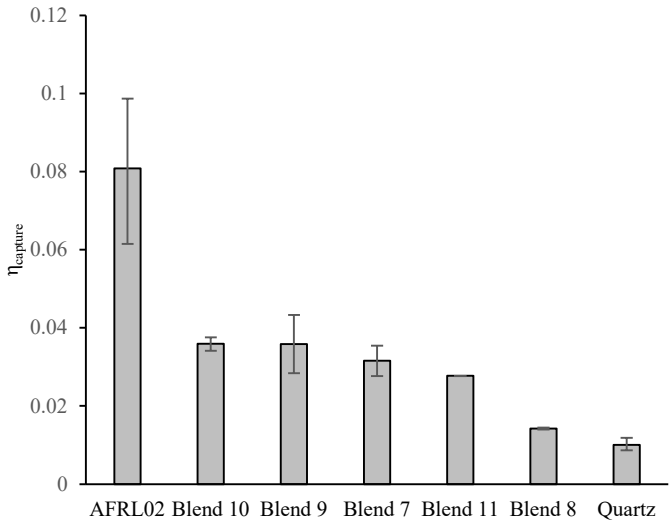

Figure 20: Simultaneous dual mineral capture efficiencies at 1144K plate surface temperature

Like the sequential results, it is confirmed that even a small amount of halite (blend 10) or dolomite (blend 9) can cause significant deposition of quartz. On the other hand, gypsum (blend 7), hematite (blend 11), and albite (blend 8), the three minerals which built large cones as a single mineral, have their deposition greatly hindered by the presence of quartz – presumably by erosion (corroborating the sequential results from Fig. 19).

In the AFRL02 deposits, two of the new minerals identified in significant quantities were diopside and wollastonite. These were previously stated to be products of quartz's reactions with dolomite and gypsum, respectively. XRD results from the simultaneous dual mineral test series confirm this (Fig. 21).

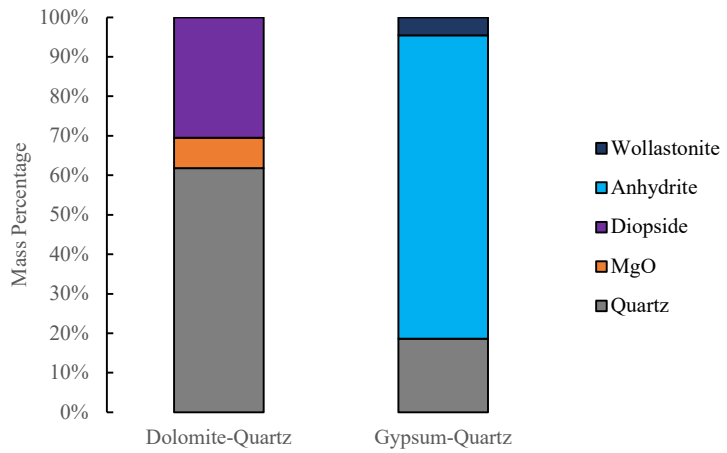

Figure 21: XRD results for blend 9 (dolomite-quartz) and blend 7 (gypsum-quartz) simultaneous dual mineral tests and plate temperature = 1144K

Blends 1-6 Tests Results

The AFRL02-like blends 1-6, defined in Table 3, were deposited at 1033K, 1144K, and 1255K plate surface temperatures. The capture efficiency results are plotted in Figure 22 alongside single mineral and AFRL02 results. The blends, plus AFRL02, are now shown in order of descending capture efficiency, according to the 1144K case. Representative photographs of each type of deposit can be found in Figure 23. XRD results for each blend-temperature combination are summarized in Table 6. For some samples, the inside and outside regions of the deposits were analyzed separately. A "$^{+}$" symbol marks minerals that usually do not contain iron in their structure, but which XRD showed containing iron with high confidence.

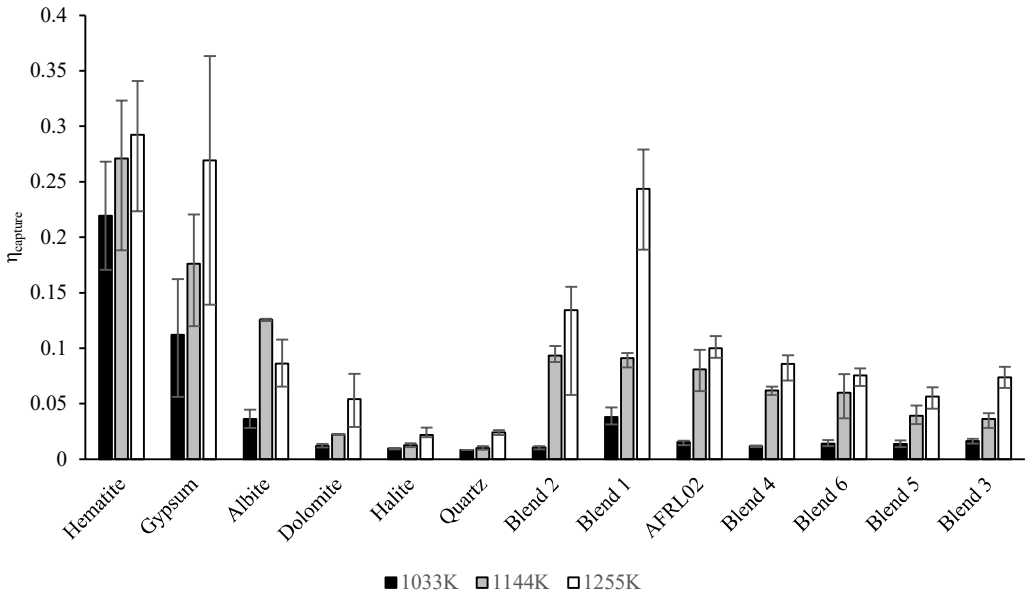

Figure 22: Capture efficiency results for all minerals and blends at all plate surface temperatures

Blend 1 (no quartz) deposited either the most or second most of all blends at all temperatures. It was the only blend to form a pointed central deposit, reminiscent of hematite, gypsum, and albite single mineral deposits. The erosive power of quartz was absent. At 1255K plate surface temperature, the presence of the blend 1 deposit caused the metal plate to overheat, and it began to melt. Also, this is the only blend where we see clear evidence of a chemical reaction with the plate by visual inspection. XRD results likewise showed with high confidence that minerals we detected in the deposit such as akermanite, brownmillerite, and pyroxferroite contained iron in their structure. The presence of iron was not surprising since the deposit's underside was black and dark green. What was surprising, however, was the formation of akermanite ($Ca_2Mg[Si_2O_7]$), since its silicon could have only come from albite.

Recall gypsum had the highest capture efficiency of the five minerals in AFRL02. As such, it would have been predicted that removing gypsum from the AFRL02 mixture would have drastically decreased the capture efficiency. Instead, at 1144K and 1255K plate temperatures, the opposite is true for blend 2. At these plate temperatures, blend 2 creates a very broad deposit, composed of 42.7% and 62.9% pure quartz, respectively. This result is even more interesting when put in perspective of the dual mineral results. Blend 8, with only albite and quartz, deposited the least. In the sequential test, quartz was found to erode albite. This suggests that the large amount of quartz in a blend 2 deposit is likely due to the presence of dolomite and halite capturing quartz.

When albite is removed from AFRL02, as in blend 3, the deposit's diameter becomes much smaller than an AFRL02 deposit. At 1033K and 1144K plate temperatures, there is practically no deposit outside the central deposit, and blend 3 had the lowest capture efficiency. At 1255K plate temperature, blend 3 is the only blend which did not melt to any observable degree. Blend 4 (no dolomite), blend 5 (no halite), and blend 7 (with hematite) all have very similar morphologies to AFRL02 at all plate temperatures.

Two general trends from the XRD results will be articulated. For gypsum-containing deposits at 1033K plate temperature, anhydrite was always the dominant depositor, comprising on average 63.9% of a deposit. Gypsum, therefore, is a danger for deposition even at low temperatures. The second trend was only possible to see by separating the central deposit from the outside regions of 1255K deposits. In all cases where this was done, a larger percentage of gypsum relative to quartz was found in the

central deposit, and, conversely, a larger percentage of quartz than gypsum was found in the outer region. This is interesting in the context of impingement flows, where there is a decline in magnitude of fluid shear as the flow moves radially outward. A higher viscosity deposit might stay confined to the stagnation region whereas a lower viscosity deposit could spread more easily to the outer regions under the influence of fluid shear.

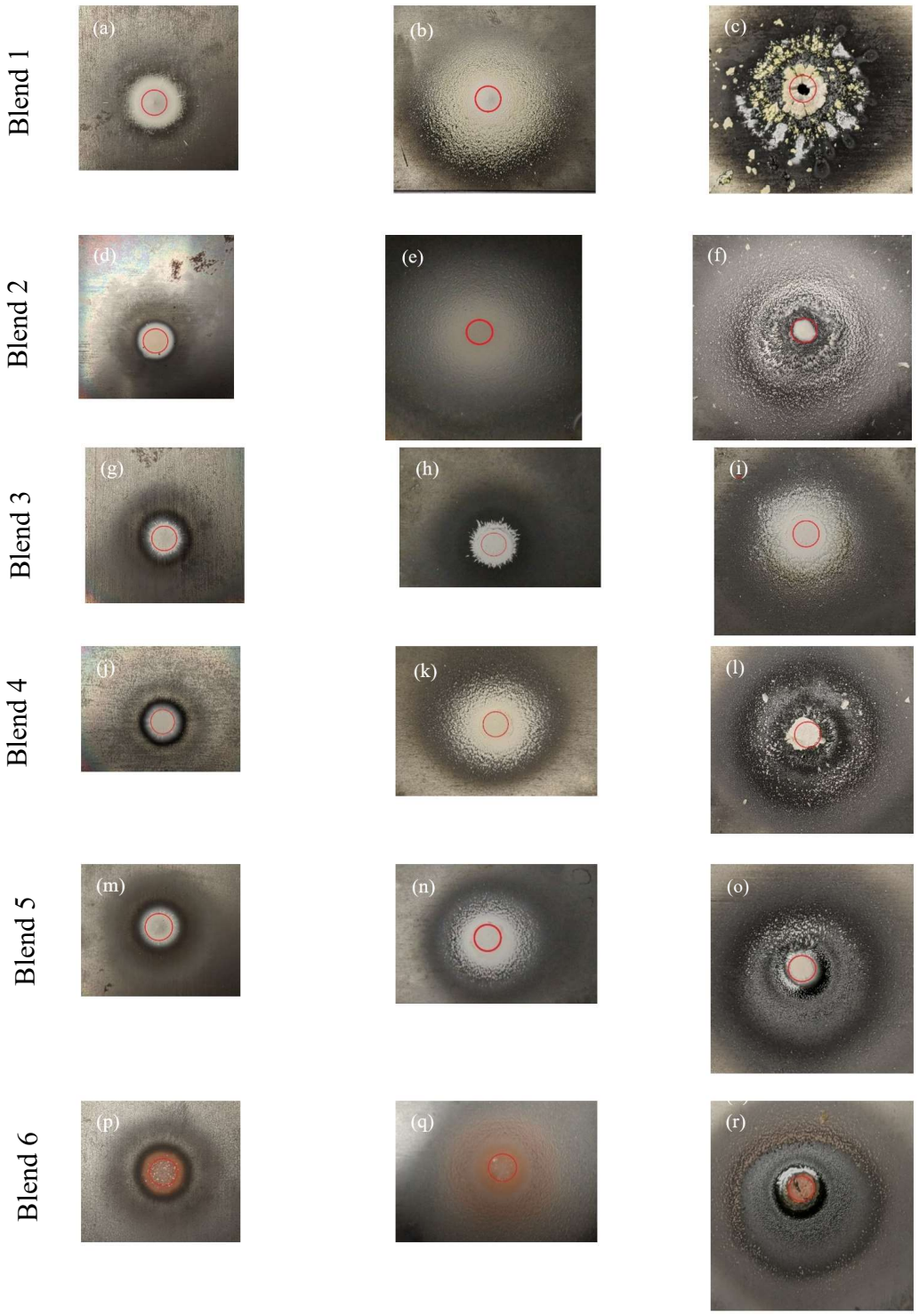

Figure 23: Representative pictures of blends' 1-6 deposits at all three plate temperatures; Column 1 = 1033K, Column 2 = 1144K, Column 3 = 1255K

Table 6: XRD results, given in weight percentage, for analyzed deposits of blends 1-6

Blend Name	1033K	1144K	1255K central	1255K outside
Blend 1	82.0% Anhydrite; 15.5% Albite; 2.5% MgO	42.8% Anhydrite; 12.8% Albite; 24.2% Melilite; 20.2% $Al_2Ca_4MgSi_3O_{14}$	43.3% Anhydrite; 15% Albite; 31.2% Akermanite; 6.5% Andalusite	15.7% Anhydrite; 48.5% Akermanite+; 15.2% Anorthite; 10.0% Brownmillerite; 7.2% Pyroxferroite; 3.4% Fe_3O_4
Blend 2	(Sample too small to analyze)	42.7% Quartz; 34.5% Albite; 22.8% Diopside	62.9% Quartz; 23.8% Albite; 13.3% Diopside	
Blend 3	28.2% Quartz; 62.7% Anhydrite; 6.7% Wollastonite; 2.4% Diopside	18.1% Quartz; 71.8% Anhydrite; 1.1% Wollastonite; 7.0% Diopside+; 2.0% Andradite;	21.2% Quartz; 29.9% Anhydrite; 24.4% Wollastonite; 13.8% Diopside; 10.7% Akermanite	41.8% Quartz; 7.6% Anhydrite; 28.6% Wollastonite; 13.1% Diopside; 8.9% Cristobalite
Blend 4	17.9% Quartz; 65.5% Anhydrite; 16.6% Albite; 1.1% Forsterite	31.9% Quartz; 17.5% Anhydrite; 20.5% Albite; 30.1% Wollastonite	20.8% Quartz; 39.8% Anhydrite; 1.6% Albite; 37.8% Wollastonite	
Blend 5	14.3% Quartz; 48.1% Anhydrite; 37.6% Albite	13.4% Quartz; 24.4% Anhydrite; 26.3% Wollastonite; 9.1% Albite; 26.8% Akermanite	22.9% Quartz; 35.4% Anhydrite; 8.6% Wollastonite; 2.9% Albite; 30.2% Diopside	

Continued

Table 6 Continued

Blend 6	17.7% Quartz; 61.2% Anhydrite; 3.9% Wollastonite; 11.3% Albite; 3.1% Diopside; 2.8% Hematite	29.6% Quartz; 29.6% Anhydrite; 6.3% Wollastonite; 20.6% Albite; 10.6% Diopside; 3.3% Hematite	31.4% Quartz; 28.5% Anhydrite; 9.5% Wollastonite^{+}; 7.0% Albite; 21.9% Diopside^{+};1.7% Hematite	53.2% Quartz; 14.1% Anhydrite; 2.2% Wollastonite; 23.3% Albite; 3.7% Diopside; 3.5% Hematite

Supplemental Studies

Two additional data sets were taken, which were generally outside of the main scope of this project, but nonetheless worth recording for posterity.

Alumina Results

Quartz played a very special role in the AFRL02 mixture above due to its propensities to erode, stick, and/or react depending on its surroundings. Quartz was also the only pure acidic oxide in this thesis. It was desired to understand if quartz's behavior was a general result for acidic oxides. Thus, Alumina (Al_2O_3), an acidic oxide, was tested twice at the 1144K plate surface temperature.

Unlike quartz, alumina deposited en masse by itself. In fact, it even captured more dust than the previous greatest-depositor of the single minerals, hematite. Similar to hematite, alumina created a very large cone, but there is little to no deposition outside of the stagnation region.

Figure 24: Representative alumina deposit at 1144K plate surface temperature

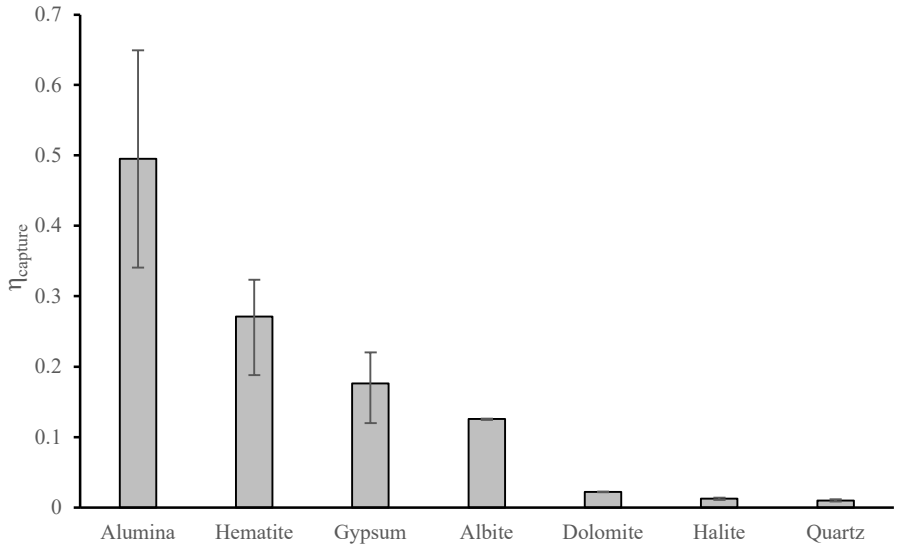

Figure 25: Single mineral capture efficiencies including alumina

ARD Results

Besides AFRL02, the other widely known test dust in the gas turbine industry is ARD, which was first introduced in Chapter 1. An ARD test series was carried out at all three plate surface temperatures according to the standard procedure. However, an additional two tests were performed at a constant 1144K plate surface temperature with a variable *flow* temperature: besides 894K, 839K and 950K flow temperatures were also tested, keeping all other variables (such as velocity of flow) constant.

ARD deposited much more than any other blend, creating a large cone, even though it contained the erosive quartz. In line with other dust blends, the deposit became molten for the 1255K plate temperature and 894K flow temperature case.

The test series performed with variable flow temperature was unique among the experiments performed for this thesis. For none of the flow temperatures, even the highest, did the deposit become molten on the 1144K plate. However, the major conclusion the data show is that capture efficiency is much more sensitive to flow temperature than plate surface temperature. The slope is much steeper for the varying flow temperature, despite of and because the change in temperature only spanned 111K for the variable flow case, whereas 222K was spanned for the change in plate case.

Figure 26: Representative pictures of ARD deposits at constant (1144K) plate surface temperature and varying (a) 839K, (b) 894K, (c) 950K flow temperature

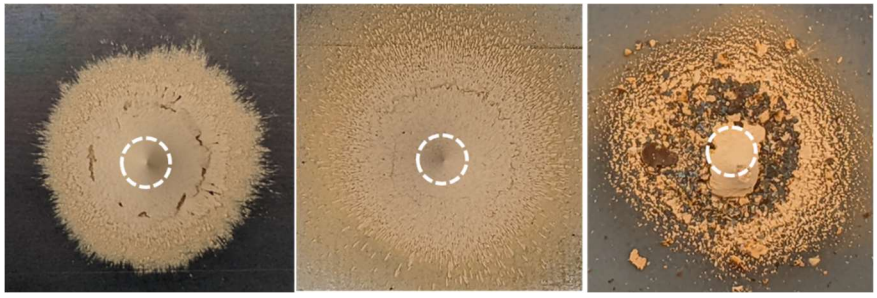

Figure 27: Representative pictures of ARD deposits at constant (894K) flow temperature and varying (a) 1033K, (b) 1144K, (c) 1255K plate surface temperature

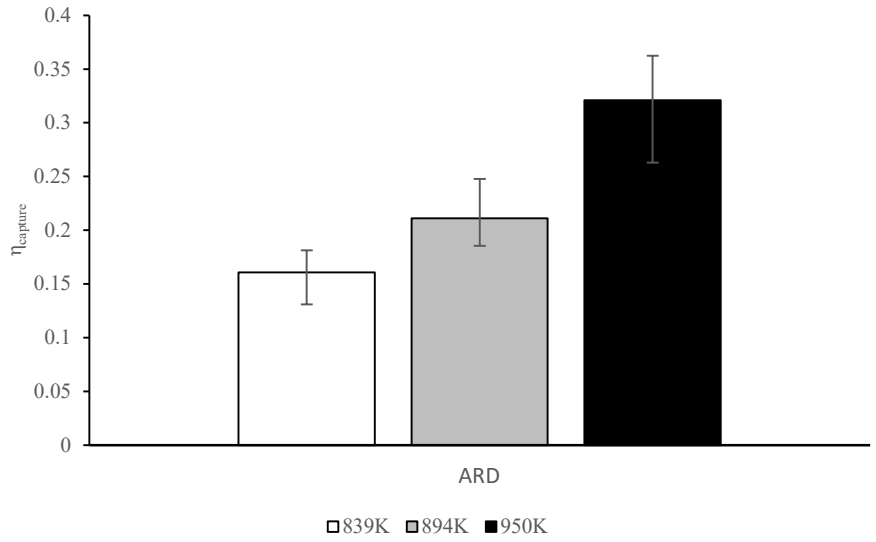

Figure 28: ARD capture efficiencies at various flow temperatures

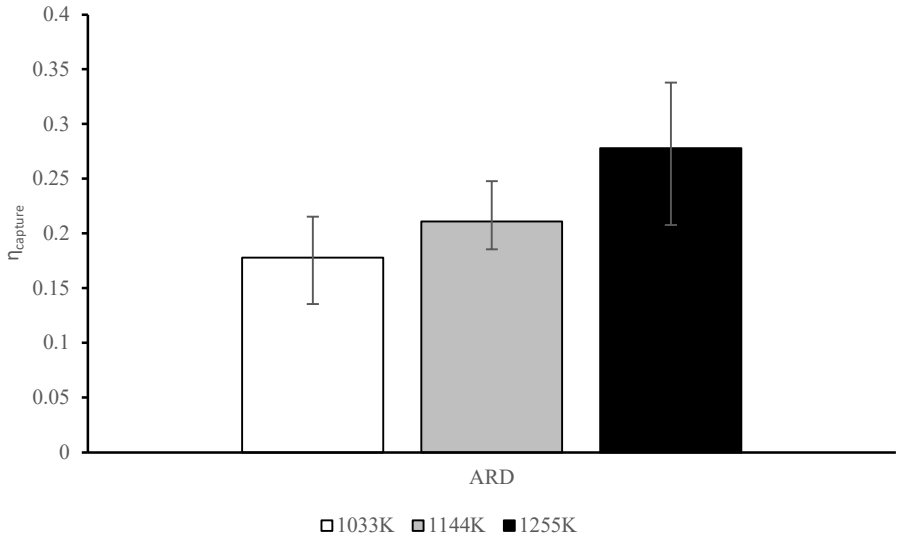

Figure 29: ARD capture efficiencies at various plate surface temperatures

XRD results will not reported in full, but general comments will be made.

Surprisingly few chemical reactions were observed compared to changes in AFRL02

deposits. This may be because the clay minerals and feldspar minerals which make up over half of ARD already contain silicate groups and are not likely to react further with quartz. Quartz probably did react with calcite. At all plate and flow temperatures, XRD revealed calcite disappeared from the samples. The mechanism was certainly very similar to that seen in dolomite – carbon dioxide is volatilized to the atmosphere leaving CaO behind. In all samples, dominant peaks belonging to the feldspars broadened, signaling formation of more glassy phases. The most dramatic changes were seen for the 1255K plate temperature, where melting was observed. RIR showed a lesser proportion of pure quartz, as opposed to other samples in which quartz deposited similarly to its original amount in the raw powder. Besides the calcite peak, one other peak at $2\theta = 19.75°$ disappeared entirely. Which mineral changed is still undetermined at the time of writing. Quartz was captured in quantities comparable to its percentage in raw ARD dust, meaning something was capturing it. Calcite is an obvious candidate. Based off of albite's interaction with quartz in AFRL02, it would seem unlikely that feldspars captured quartz. Synergies between quartz and clay minerals are unknown and should be investigated in future work.

Chapter 11: Discussion

In the above results, varying the heterogeneous mineral content of the blends had a non-trivial effect on the capture efficiencies, morphologies, and final chemical compositions of deposits. The proposed conclusion to be discussed further in this section is that chemistry of a heterogeneous dust blend is important because each mineral donates certain alkali/alkaline-earth oxides to a eutectic mixture, which ultimately determines all the properties of the final deposit, such as critical temperatures. The assertion is that minerals with lower melting temperatures naturally contribute more to deposition because their collisions with surfaces are more inelastic, they spread to maximize surface area contact, and through the addition of capillary forces and surface tension forces, which are orders of magnitude greater than just electrostatic or van der Waals forces, they are more likely to bond to a surface. However, the phases of the incoming minerals are equally important. Before combining into eutectic melts, each mineral has its own physical and chemical properties, which can impact deposition (e.g. erosion).

In this theoretical framework, all minerals in AFRL02 are divided into three groups: 1) basic oxides and their donors, 2) acidic oxides and their donors, and 3) alkali/alkaline-earth silicates and aluminosilicates. There are three basic oxide donors in AFRL02: gypsum, dolomite, and halite. In the temperature and chemical environments inside of a gas turbine engine, these minerals decompose into alkali/alkaline-earth basic

oxides and gasses. (Gasses released during these decompositions may bring with them their own problems – the outgassing of SO_3 from gypsum makes it a prime suspect for sulfur corrosion inside of the engine [50].) The second group of minerals is acidic oxides and their donors. Quartz is an acidic oxide. It has a natural affinity to react with basic oxides. Kaolinite, a common clay mineral present in ARD, would also fall into this category. It is known to spontaneously absorb alkali metals, such as sodium, into its structure [41]. Although containing both alumina and a silica, albite is not included as an acidic oxide donor, as it is already in combination with an alkali oxide and thus defines our third group, alkali/alkaline-earth silicates and aluminosilicates. Feldspars and most clay minerals (after volatizing off their hydroxide group) fall in this category, as well as silicates such as wollastonite and diopside. The contention is that "all roads lead to Rome," (Rome as a metaphor for CMAS deposits): with enough heat and time, eventually all minerals which stick in the engine will form alkali/alkaline-earth silicates/aluminosilicates, such as CMAS.

Consider the formation of diopside in the deposits. First, dolomite, a basic oxide donor, decomposes to leave CaO and MgO: $CaMg(CO_3)_2 \rightarrow CaCO_3 + MgO + CO_2$ (589K); $CaCO_3 \rightarrow CaO + CO_2$ (811K) [51]. By 1273K, CaO and MgO left over from this decomposition will react with available SiO_2 to form diopside. Despite the high melting temperatures of CaO, MgO, and SiO_2 (2845K, 3125K, and 1986K, respectively), the melting temperature of diopside is considerably lower (1665K). Dolomite decomposes into basic oxides at a lower temperature than gypsum. Any decomposition below 1473K will be minimal for gypsum [52]. Dolomite's reaction with quartz also leads to a lower

melting temperature mineral than gypsum's reaction with quartz – wollastonite melts at 1813K.

This example helps make sense of multiple results from this study. In the sequential dual mineral tests, dolomite captured quartz whereas anhydrite was slightly eroded by quartz. In simultaneous dual mineral tests, quartz was captured in both tests, but more so for the dolomite test. Both diopside and wollastonite were formed, but the amount of diopside was considerably larger. This may be because the decomposition of dolomite occurs at a lower temperature and is thus more complete and more reactive, donating more available CaO to reactions with quartz. And also because the final product of the reaction has a lower melting temperature and is thus stickier. It is hypothesized gypsum would have captured more quartz and formed more wollastonite had the experiments been run at higher temperatures still.

A second example this theory might explain is how blend 2, which lacked the highly-depositing gypsum, had an increased capture efficiency compared to AFRL02. Since gypsum does not capture quartz as efficiently as dolomite at these temperatures, its presence in AFRL02 may act to decrease the number of quartz collisions with dolomite and halite, blocking their ability to sinter and react. Additionally, collisions that *do* occur may lead to the removal of gypsum by erosion. Reactions that do occur involving gypsum and quartz occur at higher temperatures and ultimately result in relatively higher melting temperature products, which have higher viscosity and are less inclined to spread to wider regions on the plate. Therefore, the formation of lower melting temperature, wide deposits in blend 2 can be explained by the lack of gypsum. Likewise, the blend 3

deposits, which lacked the low melting temperature albite, had to form all their eutectics from basic oxides and quartz. None of the low melting temperature albite was available to promote deposition.

Alkali (alumino)silicates, such as albite, can undergo similar reactions when the more ionic magnesium and calcium oxides spontaneously move to replace Na_2O in the albite structure. The sodium is volatilized off in a gaseous state [12, 36]. MgO and CaO take its place in the crystal structure. The net effect of this type of substitution on the deposit is to raise its melting temperature, allowing calcium-containing phases to recrystallize. Blend 1's XRD results for the 1255K plate temperature case where the deposit was observed to be molten is an example of this. Despite containing no pure quartz, akermanite crystals formed in great quantities, meaning the silica from albite recombined with CaO and MgO from dolomite. Na and K feldspars and other aluminosilicates might cause more deposition in the short term because they have lower melting temperatures, but over long periods of time their Na and K will be slowly but surely replaced by Ca and Mg, leaving hardened CMAS deposits. These deposits will also have higher viscosity and surface temperatures. Pure albite on a 1255K plate rolled off the plate in liquid beads to the extent its capture efficiency decreased compared to the 1144K case. This is in contrast to blend 1's deposits at this temperature, which were also clearly molten, but wetted the surface of the metal and had a greater resistance to the shear forces of the flow.

Generalizations and Limitations

Crowe and Bons and this study have both shown one cannot predict deposition of a heterogeneous dust blend via a linear summation of single minerals' deposition behavior. As mentioned in the Literature Review, Song et al., Dunn, and Poerschke et al. all ventured to propose simple metrics based on the chemistry of basic and acidic oxides. But similar metrics in FBC which might show correlations with great success in one scenario have been shown to fail in others. This is seen in the data of this thesis. Blend 1 and blend 2 deposits had the two highest capture efficiencies of all dust blends at higher temperatures, despite the fact their deposits also had the two *most different* CaO/SiO_2 ratios among all dust blends (1.14 for blend 1 and 0.04 for blend 2 for the 1255K case).

There are two considerations that must be added when characterizing a dust's propensity for deposition: 1) One must consider mechanical effects such as the erosion of deposits. The presence of an erosive mineral would certainly skew the results of any model where erosion was not considered. Also, chemical analysis alone is not able to explain why pure alumina, hematite, and gypsum deposited so much as single minerals. The explanation must also take mechanical effects into account. 2) The second consideration is whether or not basic and acidic oxides are already combined in an alkali/alkaline-earth silicate or aluminosilicate as they enter the engine, or if they must react inside of the engine to form one. If they must react, at what temperature do basic oxide donors decompose and what is the volatile gas? What temperature does the basic oxide begin reacting with quartz? At what temperature and chemical balance will high-melting temperature calcium-containing minerals precipitate out of the melt? Treating

mechanical and chemical mechanisms in tandem and incorporating the understanding of chemical pathways an arbitrary dust blend takes to reach a CMAS melt have the potential to increase success of future predictive metrics.

An important unanswered question from this study is the time scale at which these various reactions take place. Take the case of quartz depositing on top of dolomite in the sequential dual mineral tests. Do dolomite and quartz react immediately upon contact, at time scales on the same scale as the impact time? This would suggest that chemistry is responsible for the sticking of quartz. Or is the sticking mechanism completely mechanical? Perhaps dolomite softens the surface only, allowing the collision of quartz to be more inelastic, and once in situ the two react over a time scale much greater than the impact time scale. Identifying the correct mechanism for quartz sticking to dolomite would be an important leap for this type of research.

Another Look at Factors Which Affect Deposition Through the Lens of Chemistry

It is clear that heterogeneous chemistry plays an important role in the deposition phenomenon. We next revisit the list of factors discussed in Chapter 2 and relate these back to deposit properties such as transition temperatures and thus to eutectic chemistry.

Effect of Temperature

It has been shown in this study and [14] among others that increasing the temperature of the surface at constant flow temperature increases deposition non-linearly. It has also been shown in previous studies that increasing flow temperature also increases

deposition, with perhaps a stronger dependency on flow temperature, as was certainly the case with ARD in this study. In both of these cases, the higher the temperature, the more of a chance to surpass a critical temperature. Morris [37] pointed out increased temperature increases melted fraction and decreases viscosity and surface tension in FBC agglomerates.

Why should deposition depend on temperature? Stated differently, why do things become more sticky as they become hotter? The reason is that as deposits soften and melt, they will increase the amount of inelastic collisions by absorbing the kinetic energy of incoming particles. They also spread to maximize the amount of surface contact between a mineral and a deposit. Electrostatic and van der Waals forces are very important for deposition, but if a low viscosity, molten deposit creates capillary and liquid bridge forces between particles, then these dwarf the magnitude of other forces by at least an order of magnitude. Even below the melting temperature, sintering of common edges create dominant forces holding deposits together. The important temperature-dependent properties discussed here: critical temperatures, viscosity, and surface tension are all directly related to the chemistry of the deposit.

Effect of Particle/Flow Velocity

Zhang et al.'s data showed that velocity is important because at low velocities an increase in velocity means more total delivery of particles, while at higher regimes the shear from the velocity will become erosive and decrease final capture efficiency [18]. However, flow velocity also affects the magnitude of convective heat transfer. In order

for a critical temperature to be surpassed, heat energy must be transferred to a particle. This can occur by conduction, convection, or radiation. A deposit stuck to a metal surface will conduct heat back and forth with the surface. However, when looking at a model of deposition, it is the surface of the deposit itself that is most important, because that is where new particles will collide and increase the size of the deposit. If the deposit is large, its insulating nature will make the effect of surface temperature not as immediate as the flow temperature. The velocity of the air traveling over the deposit therefore can in theory greatly affect the heat transfer. That can have competing consequences based on whether the flow is a coolant flow or hot flow. In a hot flow, one should expect the effect of this phenomenon to increase deposition with increasing flow velocity, as more heat is transferred to the surface where particles are colliding, raising the temperature of the surface and making it stickier. The opposite is true for a coolant flow: an increase in velocity will cause greater cooling of the deposit surface, and decrease deposition.

Of course, the other mechanisms of particle delivery and erosion/shear removal will still be present, so it would be difficult to isolate only the heat transfer effect, but once again we see how the effects of a variable in deposition, flow velocity, can be related back to critical temperatures and viscosity, which are related to chemistry.

Effect of Pressure

At takeoff, pressures inside a gas turbine engine can reach up to 30 atmospheres. It has been shown that increasing pressure decreased deposition in an impingement/effusion cooling geometry [30]. This is attributed to the particle following

the streamline closer due to (stokes flow). However, it is also known that chemical reactions and phase transformations are highly dependent on both temperature *and* pressure. Increased pressure during the precipitation of a mineral from a eutectic melt may result in minerals with higher or lower critical temperatures than those formed at atmospheric pressure. More research into these specific mineral reactions at relevant gas turbine pressures is needed.

Effect of Particle Size

It has been observed that smaller particles cause more deposition [22]. Larger particles move through the hot section faster. Smaller particles have a longer residency time in the combustor. Also, because of their small size, they come to thermal equilibrium faster [21]. What this adds up to is if the temperature inside the engine is above a critical temperature the smallest particles are most guaranteed to reach thermal equilibrium before impact, which maximizes the possibility of sticking.

Smaller particles were the most likely to cause deposition until a certain temperature was surpassed, after which even larger particles would deposit readily. Eutectic chemistry controls transitional temperatures, which in turn determines at which temperature the effect of size is no longer critical, and all sizes deposit.

Effect of Particle Shape

Many models model particles as spheres, which has been criticized because particles are not spheres. However, if the melting temperature of a mineral is exceeded,

the particle *will* become a sphere in stagnant air, and teardrop shaped in a moving flow. Therefore, understanding the critical temperatures (and therefore chemistry) of minerals is important because it can predict under which conditions spherical drag and impact models are valid.

Below melting temperature different mineral phases will have different shapes depending on fracture, cleavage, and crystal structure – all chemistry dependent. Minerals that break in plate-like sheets, such as muscovite, will have more drag and be less likely to impact a surface.

Dust Versus Volcanic Ash

In our experiment, all minerals were initially in crystalline phases. We did not consider the effect of adding solid, amorphous phases to the mixture. Taltavull et al. found the melting temperatures of volcanic ashes containing up to 80% amorphous phases to be dramatically reduced compared to melting temperatures of crystalline solids [53]. Wood et al. compared elemental compositions of 13 dust samples and five volcanic ash samples from around the globe. On average, volcanic ash contained slightly more silicon and aluminum than dust samples, and dust samples contained slightly more calcium than volcanic ash samples [9]. The increased silicon content in volcanic ash is one factor leading to its decreased melting temperature, but it is more likely the amorphous phases that lead to increased capture efficiency as observed by Ai and Fletcher [54]. Once again, the *phase* (in this case amorphous vs. crystalline) must be considered besides bulk chemistry alone.

Observations of Deposit Morphology

Qualitative deposit morphology was presented as a useful, *comparative* metric in which to make the claim that differences in morphologies were due to differences in heterogeneous mineral content. There are some interesting observations about deposit morphologies, outside of raw comparisons, that are worth mentioning.

Deposit Cone Growth

The dusts that formed large cones were alumina, hematite, gypsum, albite, blend 1, and ARD. Cones formed in the stagnation region of the flow. Downstream of an impingement coolant flow in an engine, these cones could be especially troublesome as their thickness will greatly insulate a surface, causing overheating. Thermal conductivity of a deposit is important, which is related to the packing factor [12]. The packing factor, being a measure of porosity, has a direct relationship with the internal structure of the deposit. Therefore, the way in which the cone forms may be important to understanding its thermal conductivity.

It was observed that cones grow layer by layer. Deposition seems to start near the base of a cone, where the plate's temperature effect is the greatest, creating a raised piece of deposit that acts as a flow blocker for incoming flow following a deposit surface. This flow carries more dust particles, which strike the deposit blocking the flow (nucleation point) and stick (propagating inwards). Over time, the net effect of this phenomenon is to

create what appears to be a wave, traveling up the cone, creating a new layer. This was often observed in PSV videos.

Figure 30: Close up of an albite deposit at 1033K plate surface temperature showing the wavefronts of layer formation

These “waves,” perpendicular to the flow direction, can be seen in Figure 24. Towards the base of the deposit, the deposit morphology appears to be parallel with the flow. This shows multiple nucleation points at the base growing upwards, before coalescing with others to form wavefront.

It was observed when ARD cones were scraped off a plate, they often broke naturally along surfaces parallel to the cone’s surface, meaning the way in which the deposits grow has a large effect on the internal structure of the deposit, which may have consequences for how deposits erode and conduct heat.

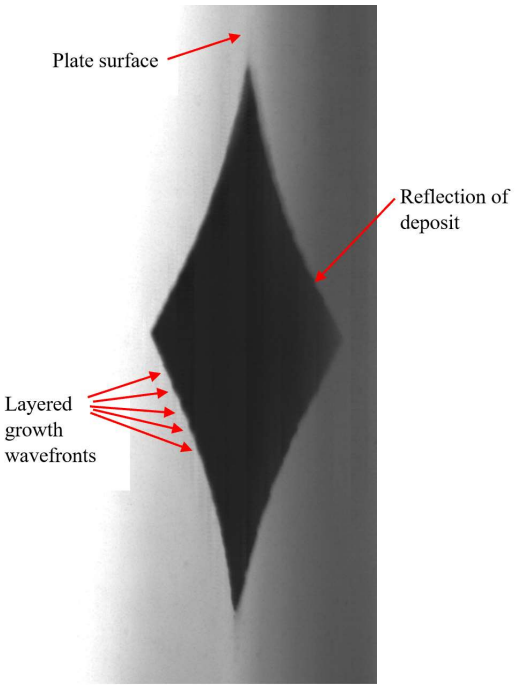

Figure 31: PSV image of albite deposit during dust delivery showing layered growth; direction of propagation is inwards, towards the peak

Figure 32: An ARD central deposit split in two, parallel to cone surface, revealing layered structure of cone

Molten Deposits

The way molten deposits acted was also very interesting. When deposits become molten, their surface tension and viscosity play an important role. Only deposits with a high surface tension and viscosity will be able to remain stuck to a surface in the face of a high shear flow. Those with lower surface tension and viscosity are more likely to wet a surface, but also likely to spread until the influence of a shear flow, which is one of Kleinhan's causes of deposit removal.

In this thesis, an example of a deposit with a low surface tension and viscosity is pure albite at the 1255K plate surface temperature case. This was the only deposit whose capture efficiency decreased at the highest temperature. In terms of our chemical theory, this makes sense, as albite does not contain calcium. Also, it contains a high proportion of silica compared to alkali metal. An example of a deposit with a high surface tension and viscosity is blend 1 at 1255K plate surface temperature. In contrast to pure albite, this deposit contains a much higher amount of calcium, and would therefore be hypothesized to have a much higher surface tension, melting temperature, and viscosity. Indeed, even though the blend 1 deposit was clearly molten (and even had droplets escape the stagnation region under the influence of shear flow), it was still able to increase its capture efficiency greatly with a rise in surface temperature.

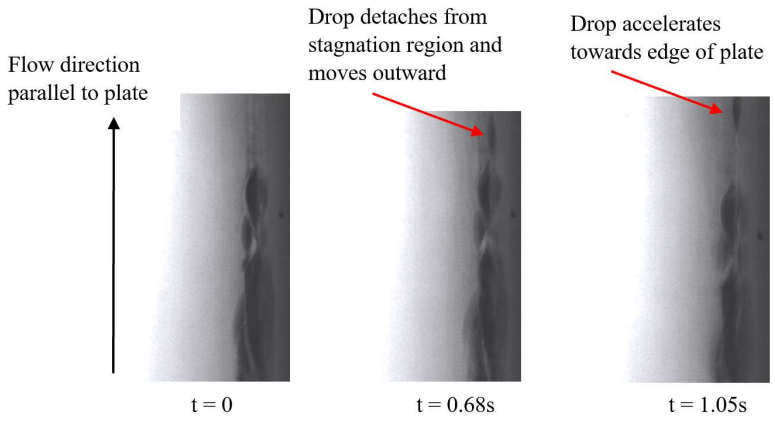

Figure 33: A molten drop detaches from central deposit and moves outwards under influence of shear flow

Molten material in deposits might also be responsible for the speckled region seen in AFRL02 and other deposits. A molten layer closest to the plate gives a low-viscosity medium over which any chunks of deposit breaking off from the central deposit could slide and reattach at outside regions where the temperature might have lowered again. Despite capture efficiency increasing with temperature, it is curious that the largest deposits seen in Fig. 2 are near the coolant holes. Molten deposit could have built up in stagnation regions, spread upon molten layers, and reattached where cooling was greatest.

The Gap Region

The gap region was introduced above. It is typically a region just outside the stagnation region, in which little to no deposition occurs, in stark contrast to the stagnation region and the halo region. Its existence is interesting because it suggests some

condition or combination of conditions in that region make deposition highly unfavorable. A few mechanisms have been proposed for its formation: 1) heat transfer may be particularly high there, causing the surface in just that ring to be cool enough to be below a threshold temperature for deposition. As the flow moves outward on the plate, however, it picks up heat from the plate so that heat transfer in the outer regions is not as efficient. 2) In the free flow region of an impingement jet, Kelvin-Helmholtz instabilities have been known to form from shear between the free jet and the surrounding atmosphere [55]. These vortices can create regions of high velocity/circulating flow, which makes deposition unfavorable. 3) Particles with a sufficiently high Stokes number will be unable to turn with the flow and will impact the stagnation region. However, the sticking efficiency of these is not perfect and some particles will bounce off the plate/deposit and reenter the flow. It is possible that these rebounded particles collide downstream with the plate a second, third, etc. time and can stick on these subsequent impacts. This process could be complicated, but it is possible the gap region is due to the rebounding kinetic energy of particles being high enough to skip the region adjacent to the stagnation region, thus creating a gap.

In the case of AFRL02 and similar blends at 1255K, it was pointed out what appeared like a gap was actually just a gap in speckled deposits, and a thin, glassy layer spread over the entire region of the deposit. The speckles might have broken off from the central deposit as large pieces and glided under the influence of shear about this low-viscosity molten layer, finally settling when attractive forces between speckled deposit and plate balanced the force of shear.

Deposit Erosion

Erosion is a very important factor in deposition for many reasons. For one, the existence of erosion may cause underprediction of deposition in models. Erosion also has the ability to be used as a tool to combat deposits mid-air. The author of this thesis was once told by Dr. Michael Dunn that pilots who had flown through a cloud of volcanic ash were advised to lower the temperature of their engines temporarily (slow down) so that deposits could be eroded off through thermal stresses. Kleinhans et al. identified three modes of deposit removal (or erosion) in deposition in coal combustion systems [12]. 1) shedding of deposits due to mechanical stresses; 2) erosion caused by sharp, non-molten particles colliding with a deposit; and 3) deposits with low viscosity/surface tension dripping off a surface [12]. All three mechanisms have been observed in this work: 1) While cooling to room temperature, central deposits of AFRL02 and other blends cracked and/or sputtered off the plate surface because of a mismatch in coefficients of thermal expansion; 2) Quartz eroded deposits of albite and other blends; and 3) pure albite was the only dust whose capture efficiency did not monotonically increase because liquid albite spread off the edges of the plate.

Chapter 12: Conclusions

Experiments were performed to determine the effect of varied mineral dust composition on deposition in an impingement coolant flow at three metal surface temperatures relevant to gas turbine engines.

Conclusion 1: Deposition of single minerals cannot predict heterogeneous dust deposition.

Deposits were characterized in three ways: capture efficiency, morphology, and XRD. In all three ways, knowledge of single mineral deposition behavior failed to consistently predict blends' deposition behavior.

Conclusion 2: Deposition of quartz is interesting and important.

Deposition of quartz is important to understand in the field of particle deposition in gas turbine engines due to its prevalence in the earth's crust, regardless of region. It was shown quartz is also important because of its interactions with other minerals. Quartz showed the capability to erode albite deposits and likely other blends' deposits as well. Nevertheless, it deposited significantly in every mineral blend when present. Not only did

it deposit, but it reacted with basic oxides to form new minerals with melting temperatures considerably lower than quartz'. Thus, quartz can be both erosive and/or acidic oxide fodder for reactions with basic oxides.

Conclusion 3: Capture efficiencies of heterogeneous dust blends all increased with temperature, but not according to the same trend.

The capture efficiency of all single minerals and blends increased with increasing plate surface temperature. However, the trends were not always linear or consistent between blends. The only exception was albite at 1255K plate surface temperature, whose capture efficiency decreased compared to the 1144K case, due to the low viscosity melt running off the plate.

Conclusion 4: When considering chemistry's effect on deposition, consider the phases as they enter the engine instead of just total oxide composition.

Temperatures of decomposition, reaction, melting, and recrystallization vary broadly for different minerals. Minerals entering the engine as low temperature eutectics do not need additional heat energy to drive a chemical reaction; they can soften or melt directly. Even calcium containing minerals are still candidates for erosion by quartz if the temperature inside the engine is not high enough to instead drive their reaction *with* quartz. This conclusion should be extended to amorphous vs. crystalline phases as well.

References

[1] Hileman, J.I., Stratton, R.W. and Donohoo, P.E., 2010. “Energy content and alternative jet fuel viability.” *Journal of propulsion and Power*, *26*(6), pp.1184-1196.

[2] Harkins, G., 2015. “Pilot missteps, brownout led to Hawaii Osprey crash.” *Marine Corps Times,* viewed March 29, 2022, < https://www.marinecorpstimes.com/news/your-marine-corps/2015/11/23/pilot-missteps-brownout-led-to-hawaii-osprey-crash/>

[3] Kelly, F., 2017. “V-22 Osprey hard landing injures 2 US service members in Middle East.” *The Defense Post*, viewed March 29, 2022, < https://www.thedefensepost.com/2017/09/29/v-22-osprey-crash-syria-us-injured/>, image: U.S. Marine Corps/Lance Cpl. Becky L. Calhoun.

[4] Chambers, J.C., 1985, “The 1982 Encounter of British Airways 77 with the Mt. Galuggung Eruption Cloud,” AIAA Paper 85-0097.

[5] Cumpsty, N., 2003. *Jet Propulsion: A Simple Guide to the Aerodynamic and Thermodynamic Design and Performance of Jet Engines*. 2nd ed., Cambridge UK: Cambridge University Press, 2003.

[6] Yin, Y., Wurzler, S., Levin, Z. and Reisin, T.G., 2002. “Interactions of mineral dust particles and clouds: Effects on precipitation and cloud optical properties.” *Journal of Geophysical Research: Atmospheres*, *107*(D23), pp.AAC-19.

[7] Gutro, R., 2020. “NASA Observes Large Saharan Dust Plume Over Atlantic Ocean.” NASA, viewed March 29, 2022, <https://www.nasa.gov/feature/goddard/2020/nasa-observes-large-saharan-dust-plume-over-atlantic-ocean.>

[8] Christian, J., 2020, Agence France Presse, viewed March 30, 2022 on < https://www.bbc.com/news/in-pictures-55173480>

[9] Wood, C.A., et al., 2017, "Characterisation of Dirt, Dust and Volcanic Ash: A Study on the Potential for Gas Turbine Engine Degradation." DST-Group-TR-3367

[10] Merrill, L., 2014. “Arizona Test Dust pounds new F-150s into shape.” AZCentral, viewed March 29, 2022, <https://www.azcentral.com/story/money/business/2014/03/31/arizona-test-dust-pounds-new-f-shape/7118591/>

[11] Phelps, A.W. and Pfledderer, L., 2015, "Development of a naturalistic test media for dust ingestion CMAS testing of gas turbine engines" in *Thermal Barrier Coatings IV*, U. Schulz, German Aerospace Center; M. Maloney, Pratt & Whitney; R. Darolia, GE Aviation (retired) Eds, ECI Symposium Series. <http://dc.engconfintl.org/thermal_barrier_iv/29>

[12] Kleinhans, U., Wieland, C., Frandsen, F.J. and Spliethoff, H., 2018. “Ash formation and deposition in coal and biomass fired combustion systems: Progress and challenges in the field of ash particle sticking and rebound behavior.” *Progress in energy and combustion science*, *68*, pp.65-168.

[13] Crowe, E.D. and Bons, J.P., 2019, “Effects of Dust Composition on Particle Deposition in an Effusion Cooling Geometry,” presented at the IGTI 2019 in Phoenix, AZ, 17-21 June 2019 (GT2019-91032)

[14] Whitaker, S.M., Lundgreen, R.K., and Bons, J.P., 2017, "Effects of Metal Surface Temperature on Deposition-Induced Flow Blockage in a Vane Leading Edge Cooling Geometry." In *Turbo Expo: Power for Land, Sea, and Air*, Vol. 50817

[15] Plewacki, N., Gnanaselvam, P. and Bons, J.P., 2020. “The Effect of Elevated Temperatures on Airborne Particle Deposition and Rebounds.” In *AIAA Scitech 2020 Forum* (p. 1576).

[16] Clark, R.A., Plewacki, N., Gnanaselvam, P., Bons, J.P. and Viswanathan, V., 2021. “The Effect of Thermal Barrier Coating Surface Temperature on the Adhesion Behavior of CMAS Deposits.” *Journal of Turbomachinery*, *143*(4).

[17] Jain, N., Le Moine, A., Chaussonnet, G., Flatau, A., Bravo, L., Ghoshal, A., Walock, M.J., Murugan, M. and Khare, P., 2021. “A critical review of physical models in high temperature multiphase fluid dynamics: Turbulent transport and particle-wall interactions.” *Applied Mechanics Reviews*, *73*(4).

[18] Zhang, F., Liu, Z., Liu, Z. and Liu, Y., 2019. “Experimental study of particle deposition on surface at different mainstream velocity and temperature.” *Energies*, *12*(4), p.747.

[19] Bowen, C.P., Libertowski, N.D., Mortazavi, M. and Bons, J.P., 2018, June. "Modeling deposition in turbine cooling passages with temperature dependent adhesion and mesh morphing." In *Turbo Expo: Power for Land, Sea, and Air* (Vol. 51029, p. V02DT47A009). American Society of Mechanical Engineers.

[20] Singh, S. and Tafti, D., 2015. "Particle deposition model for particulate flows at high temperatures in gas turbine components." *International Journal of Heat and Fluid Flow*, *52*, pp.72-83.

[21] Bojdo, N. and Filippone, A., 2019. "A simple model to assess the role of dust composition and size on deposition in rotorcraft engines." *Aerospace*, *6*(4), p.44.

[22] Whitaker, S.M., Peterson, B., Miller, A.F. and Bons, J.P., 2016, June. "The effect of particle loading, size, and temperature on deposition in a vane leading edge impingement cooling geometry." In *Turbo Expo: Power for Land, Sea, and Air* (Vol. 49798, p. V05BT16A013). American Society of Mechanical Engineers.

[23] Wolff, T., Bowen, C. and Bons, J.P., 2018. "The effect of particle size on deposition in an effusion cooling geometry." In *2018 AIAA Aerospace Sciences Meeting* (p. 0391).

[24] Crosby, J.M., Lewis, S., Bons, J.P., Ai, W. and Fletcher, T.H., 2008. "Effects of temperature and particle size on deposition in land based turbines." *Journal of Engineering for Gas Turbines and Power*, *130*(5).

[25] Bonilla, C., Webb, J., Clum, C., Casaday, B., Brewer, E. and Bons, J.P., 2012. "The effect of particle size and film cooling on nozzle guide vane deposition." *Journal of engineering for gas turbines and power*, *134*(10).

[26] Bons, J.P., Prenter, R. and Whitaker, S., 2017. "A simple physics-based model for particle rebound and deposition in turbomachinery." *Journal of Turbomachinery*, *139*(8).

[27] Connolly, B.J., Loth, E. and Smith, C.F., 2020. "Shape and drag of irregular angular particles and test dust." *Powder Technology*, *363*, pp.275-285.

[28] Bowen, C.P., 2021. *Improving Deposition Modeling Through an Investigation of Absolute Pressure Effects and a Novel Conjugate Mesh Morphing Framework* (Doctoral dissertation, The Ohio State University).

[29] Weiler, C., 2008, *Generierung leicht dispergierbarer Inhalationspulver mittels Sprühtrocknung*, [*Generation of easily dispersible inhalation powder using spray drying*], (Doctor of Science, Pharmaceutical technology dissertation, Department of Chemistry, Pharmacy and Earth Sciences, Johannes Gutenberg University).

[30] Brown, C.P. and Bons, J.P., 2020, September. “An Experimental and Computational Investigation of Absolute Pressure Effects on Deposition in an Effusion Cooling Geometry.” In *Turbo Expo: Power for Land, Sea, and Air* (Vol. 84072, p. V02BT34A014). American Society of Mechanical Engineers.

[31] Sacco, C., Bowen, C., Lundgreen, R., Bons, J.P., Ruggiero, E., Allen, J. and Bailey, J., 2017, June. “Dynamic Similarity in Turbine Deposition Testing and the Role of Pressure.” In *Turbo Expo: Power for Land, Sea, and Air* (Vol. 50817, p. V02DT48A021). American Society of Mechanical Engineers.

[32] Lundgreen, R.K., 2017, June. “Pressure and Temperature Effects on Particle Deposition in an Impinging Flow.” In *Turbo Expo: Power for Land, Sea, and Air* (Vol. 50817, p. V02DT48A018). American Society of Mechanical Engineers.

[33] Song, W., Lavallee, Y., Hess, K-U, Kueppers U., Cimarelli, C., and Dingwell, D.B., 2016, “Volcanic ash melting under conditions relevant to ash turbine interactions.” *Nature Communications,* 7:10795 doi: 10.1038/ncomms10795 (2016)

[34] Veit, U., and Rüssel, C., 2017, "Viscosity and liquidus temperature of quaternary glasses close to an eutectic composition in the CaO–MgO–Al2O3–SiO2 system," *Journal of Materials Science* 52.13 (2017): 8280-8292

[35] Dunn, M.G., 2012, “Operation of Gas Turbine Engines in an Environment Contaminated with Volcanic Ash,” *Journal of Turbomachinery*, Sept 2012, 134(5): 051001

[36] Poerschke, D.L., Jackson, R.W., and Levi, C.G., 2017, "Silicate deposit degradation of engineered coatings in gas turbines: progress toward models and materials solutions," *Annual Review of Materials Research 47* (2017): 297-330

[37] Morris, J.D., et al., 2018, "Mechanisms and mitigation of agglomeration during fluidized bed combustion of biomass: A review," *Fuel* 230 (2018): 452-473

[38] Hurskainen, M., and Vainikka, P., 2016, "Technology options for large-scale solid-fuel combustion," *Fuel Flexible Energy Generation*, Woodhead Publishing, 177-199

[39] Khadilkar, Aditi B., 2016, “Development of a fluidized bed agglomeration modeling methodology to include particle-level heterogeneities in ash chemistry and granular physics,” (Doctoral dissertation, The Pennsylvania State University)

[40] Vassilev, S.V., Baxter, D., and Vassileva, C.G., 2013, "An overview of the behaviour of biomass during combustion: Part I. Phase-mineral transformations of organic and inorganic matter," *Fuel* 112 (2013): 391-449

[41] Magda, A., 2012. *Modelling of mineral matter transformation and deposition in furnaces.*

[42] Eliaz, N., Shemesh, G. and Latanision, R.M., 2002. "Hot corrosion in gas turbine components." *Engineering failure analysis*, *9*(1), pp.31-43.

[43] Han, B. and Goldstein, R.J., 2001. "Jet-impingement heat transfer in gas turbine systems." *Annals of the New York Academy of Sciences*, *934*(1), pp.147-161.

[44] Zuckerman, N. and Lior, N., 2005. "Impingement heat transfer: correlations and numerical modeling." *J. Heat Transfer*, *127*(5), pp.544-552.

[45] Gnanaselvam, P., Lo, C.H., Han, J., and Bons, J.P., 2021, "Turbulent Dispersion and Deposition of Micron-Sized Particles in a Turbulent Pipe Flow at High Temperatures," presented at the AIAA SciTech 2021 (virtual), January 2021. Paper #: AIAA-2021-0850

[46] 'Bragg's Law' (2021). *Wikipedia,* viewed March 29, 2022, <https://en.wikipedia.org/wiki/Bragg%27s_law>, image by Hydrargyrum - Own work, CC BY-SA 3.0, https://commons.wikimedia.org/w/index.php?curid=17543875

[47] Cranmer, D., and Uhlmann, D.R., 1981, "Viscosity of liquid albite, a network material." *Journal of Non-Crystalline Solids* 45.2 (1981): 283-288

[48] Babushkin, V., Matveyev, G., and Mchedlov-Petrossyan, O., 1985, *Thermodynamics of Silicates*, Springer-Verlag. 4th edition. Translated by Frenkel, B.N., and Terettyevs, V.A., New York, Pgs95-102

[49] Elms, J., Pawley, A., Bojdo, N., Jones, M., and Clarkson, R., 2020, "The Formation of High Temperature Minerals from an Evaporite-Rich Dust in Gas Turbine Engine Ingestion Tests," presented at the 2020 IGTI, paper #GT2020-14236.

[50] Krisak, M.B., et al., 2017, "Review of calcium sulfate as an alternative cause of hot corrosion," *Journal of Propulsion and Power* 33.3 (2017): 697-703.

[51] Olszak-Humienik, M. and Jablonski, M., 2015, "Thermal behavior of natural dolomite," *Journal of Thermal Analysis and Calorimetry*, 119:2239–2248

[52] Yan, Z., et al., 2015, "Decomposition and solid reactions of calcium sulfate doped with SiO2, Fe2O3 and Al2O3," *Journal of analytical and applied pyrolysis*, 113 (2015): 491-498.

[53] Taltavull, C., Dean, J. and Clyne, T.W., 2016. "Adhesion of volcanic ash particles under controlled conditions and implications for their deposition in gas turbines." *Advanced Engineering Materials*, *18*(5), pp.803-813.

[54] Ai, W., and Fletcher, T.H., 2009, "Computational Analysis of Conjugate Heat Transfer and Particulate Deposition on a High Pressure Turbine Vane," presented at ASME Turbo Expo 2009: Power for Land, Sea, and Air. June, 2009, Florida, United States. Paper #: GT2009-59573.

[55] Violato, D., Ianiro, A., Cardone, G. and Scarano, F., 2012. "Three-dimensional vortex dynamics and convective heat transfer in circular and chevron impinging jets." *International Journal of Heat and Fluid Flow*, *37*, pp.22-36.